# Is biological productivity enhanced at the New England shelfbreak front?

Weifeng G. Zhang,[1] Dennis J. McGillicuddy Jr.,[1] and Glen G. Gawarkiewicz[1]

[1]   A two-dimensional (cross-shelf) numerical model of the mean seasonal circulation offshore of southern New England predicts upwelling at the shelfbreak front. Expected ramifications of this upwelling include enhancement of nutrient supply, phytoplankton biomass, and productivity. However, seasonal climatologies of chlorophyll based on both in situ data and satellite observations show no mean enhancement at the front. We investigate this apparent discrepancy with a four-component planktonic ecosystem model coupled to the two-dimensional physical model. Nutrient fields are restored to climatological values at depth, and upper ocean values evolve freely according to physical and biological forcing. Vertical diffusivity is based on seasonally averaged surface and bottom mixed layer depths compiled from in situ observations. The model reproduces the general pattern of the observed cross-shelf and seasonal variations of the chlorophyll distribution. It predicts a local enhancement of phytoplankton productivity at the shelfbreak in spring and summer as a result of the persistently upwelled nutrient-rich slope water. In the model, zooplankton grazing prevents accumulation of phytoplankton biomass at the site of the upwelling. The predicted enhancement of primary productivity (but not phytoplankton biomass) at the shelfbreak constitutes a hypothesis that could be tested in the future with suitable measurements from regional long-term observatories, such as the Ocean Observatories Initiative Pioneer Array.

## 1. Introduction

[2]   The Middle Atlantic Bight (MAB; Figure 1) continental shelf is part of the U.S. northeast shelf that is one of the most productive large marine ecosystems of the world [*O'Reilly and Zetlin*, 1998; *Sherman et al.*, 2002]. It contributes substantially to the regional economy through commercial fishing [*Sherman et al.*, 1996a]. The ecosystem is nourished by high concentrations of phytoplankton, which undergoes substantial variation over broad spatial and temporal scales [*Marra et al.*, 1982; *Walsh et al.*, 1978; *Walsh et al.*, 1988b; *Yoder et al.*, 2001]. Analyses of historical in situ and satellite observations in the region have portrayed a general pattern of high chlorophyll concentration in nearshore regions and a decreasing trend in the offshore direction [*O'Reilly and Zetlin*, 1998; *Yoder et al.*, 2002]. The chlorophyll concentration also varies temporally with generally high concentration on the shelf in winter and in the shelfbreak and slope sea regions in spring [*Xu et al.*, 2011; *Yoder et al.*, 2002].

[3]   The MAB continental shelf contains a persistent thermohaline shelfbreak front [*Houghton et al.*, 2009; *Linder and Gawarkiewicz*, 1998] that separates the highly productive shelf region from the open ocean. Large horizontal and vertical gradients in water properties are associated with the shelfbreak front. Cross-shelf fluxes of heat, salt, nutrients, and carbon between the continental shelf and the slope sea affect the characteristics of water masses and biological production both at the shelfbreak and in the neighboring continental shelf and slope seas [*Flagg et al.*, 1994; *Houghton and Marra*, 1983; *Malone et al.*, 1983; *Vaillancourt et al.*, 2005]. Surface and subsurface enhancement of chlorophyll at the MAB shelfbreak has been observed in synoptic in situ and satellite measurements [*Marra et al.*, 1982; *Ryan et al.*, 1999a], and such enhancement could be the cause of the aggregation of some higher trophic-level species [*CETAP*, 1982] and elevated fishing activities along the shelfbreak [*Orphanides and Magnusson*, 2007; *Podesta et al.*, 1993]. However, chlorophyll levels are not always enhanced at the shelfbreak [*Hales et al.*, 2009], and chlorophyll levels at the shelfbreak are subject to the influences of frontal instability and external forcing (e.g., wind and warm-core rings) [*Hales et al.*, 2009; *Ryan et al.*, 1999b].

[4]   The New England shelfbreak region (Figure 1 inset) is a crucial part of the interface between the MAB continental shelf and the open ocean and also connects the immediate upstream, the highly productive Georges Bank, with the rest of the MAB shelf. The New England shelfbreak region has been the subject

---

[1]Woods Hole Oceanographic Institution, Woods Hole, Massachusetts, USA.

Corresponding author: W. G. Zhang, Woods Hole Oceanographic Institution, 266 Woods Hole Rd., MS# 12 Woods Hole, MA 02543, USA. (wzhang@whoi.edu)
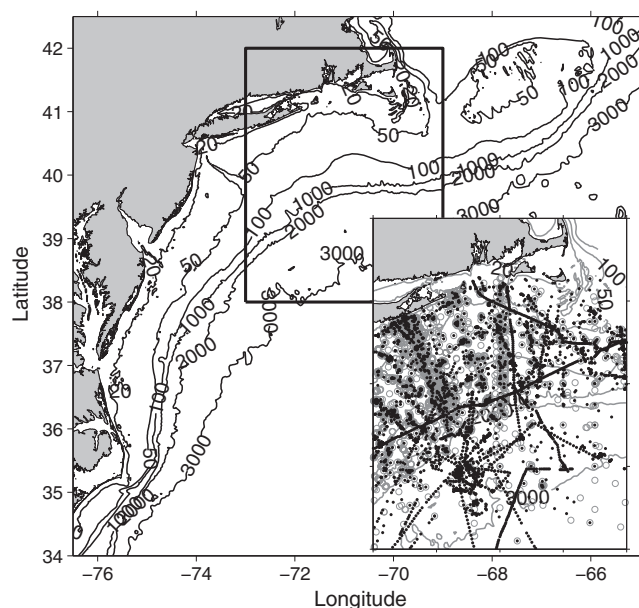
**Figure 1.** The Middle Atlantic Bight with bathymetric contours in meters. The black frame indicates the area over which historical in situ observations are averaged to produce the cross-shelf nutrient and phytoplankton climatology. The grey circles and black dots in the inset indicate the locations of the in situ nutrient and chlorophyll profiles, respectively.

of numerous observational studies[*Gawarkiewicz et al.*, 2004; *Hales et al.*, 2009; *Houghton et al.*, 2006; *Ledwell et al.*, 2004; *MacKinnon and Gregg*, 2005; *Marra et al.*, 1990; *Marra et al.*, 1982; *Pickart*, 2000; *Walsh et al.*, 1988a]. Models have been used to examine various aspects of the planktonic ecosystem and biogeochemistry in this area, ranging from detailed investigations of the shelfbreak front [*He et al.*, 2011; *Siedlecki et al.*, 2011] to larger-scale, coast-wide studies [*Fennel et al.*, 2006; *Hofmann et al.*, 2011]. However, because shelfbreak processes are inherently nonlinear and exhibit variations over a broad range of spatial and temporal scales, much of the circulation and ecosystem dynamics at the New England shelfbreak are still unknown. The ongoing construction of the Ocean Observatories Initiative (OOI) Pioneer Array [*Consortium for Ocean Leadership*, 2010] will provide unprecedented long-term and detailed observations of the ocean conditions in the area.

[5] In an idealized study of frontal dynamics at the shelfbreak, *Zhang et al.* [2011] used a 2-dimensional (2-D; cross-shelf and vertical) model in conjunction with seasonal temperature and salinity climatologies and velocity observations to study the mean circulation. One distinct feature of the model result was persistent shelfbreak upwelling that originated mostly from the upper continental slope, which was strongest in winter and fall (Figures 2e–2h). Persistent upwelling would tend to bring nutrients into the euphotic zone and thereby stimulate local biological production when the near-surface production is nutrient limited. However, because the associated vertical velocity is weak in spring and summer (~0.2 m d$^{-1}$ at 50 m depth), the degree to which the seasonal mean upwelling can enhance local productivity is unclear.

[6] In order to understand the impact of this upwelling on the seasonal mean biological production in the shelfbreak

region, a four-component planktonic ecosystem model is applied to the 2-D physical model of *Zhang et al.* [2011]. The modeled nutrient fields are restored to climatological mean values, and the predicted phytoplankton distributions are compared with both in situ and satellite-based seasonally averaged chlorophyll observations. The results of this study illuminate some of the physical and biological processes that are important for long-term seasonal mean productivity, and provide the baseline for future studies of shelfbreak ecosystem dynamics on synoptic scales.

[7] Of course the 2-D model of the climatological mean seasonal cycle is incomplete. To begin with, the 2-D formulation does not explicitly represent 3-D effects such as cross-shelf eddy fluxes or along-shelf advection. However, some of their net effects are accounted for, insofar as the model is nudged toward observations of temperature, salinity, and nutrients. The more fundamental issue is whether or not a 2-D cross-shelf model is a useful abstraction of the natural system. We argue that it is, based on a long history of 2-D conceptualizations of such systems in theoretical, observational, and numerical studies [e.g., *Barth et al.*, 1998; *Lentz*, 2008; *Siedlecki et al.*, 2011; *Wroblewski*, 1977].

[8] The simple four-compartment nutrient-phytoplankton-zooplankton-detritus model utilized herein is also highly simplified. However, it contains enough dynamics to address the process of interest, namely the impact of mean upwelling at the shelfbreak front on plankton productivity. More complex models with explicit community structure are also valid—but those additional complexities are not necessarily required to answer the specific questions posed herein.

[9] A final caveat concerns the space and time scales of variability. The shelfbreak front is a highly variable system in which standard deviations of a given property can be as large as the mean. However, as we will show in the chlorophyll climatologies constructed below, there is a statistically significant mean seasonal cycle that needs to be explained. Of course it is possible that high frequency phenomena and 3-D effects can contribute to this mean signal, but we are asking a simpler question: can the mean seasonal cycle be explained by a 2-D model with climatological forcing? In essence, the simple model constitutes a null hypothesis that we wish to test. Identification of a model solution that is consistent with the observations tells us that we cannot reject the hypothesized 2-D dynamics as an explanation for why mean productivity at the front is enhanced, whereas mean chlorophyll is not.

## 2. Methods

### 2.1. Climatologies

#### 2.1.1. Chlorophyll Climatology from Satellite Observations

[10] We computed seasonal mean surface chlorophyll concentrations in the MAB region (Figure 3) from the existing monthly chlorophyll climatology that is based on 8 years (2002–2010) of MODIS observations (http://oceancolor.gsfc.nasa.gov/). Similar seasonal mean chlorophyll distributions are evident in the 14 year SeaWiFS climatology (not shown). Seasons are defined as follows: winter is January to March, spring April to June, summer July to September, and fall October to December.

[11] In order to compare the satellite chlorophyll climatology to in situ and modeled cross-shelf chlorophyll distributions
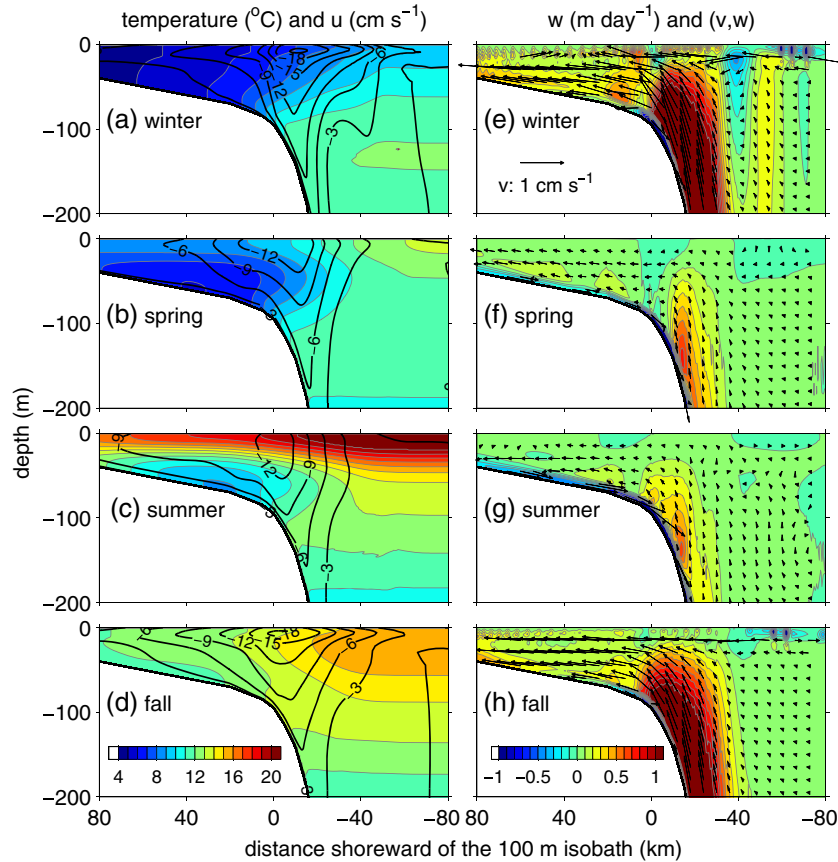
**Figure 2.** Cross-shelf sections of 2-D temperature climatology (color shading in the left column) and model along-shelf (black contour, a–d) and vertical (color shading, e–h) velocities. Vectors in the right column indicate cross-shelf and vertical velocity. The scale in Figure 2e is for cross-shelf velocity.

(see section 2.1.2 for the processing of the in situ data), we averaged the MODIS satellite chlorophyll on the New England shelf (Figure 1 inset) in the along-shelf direction and produced the mean cross-shelf distribution (red lines in Figure 4). Along-shelf averaging of the satellite chlorophyll data was carried out in a depth-binned manner with 2.5 m bottom depth intervals. For instance, all chlorophyll climatology values in the bottom depth range of 78.75–81.25 m were averaged to obtain the mean value at a bottom depth of 80 m. This method is consistent with the along-shelf averaging of temperature and salinity in *Zhang et al.* [2011].

### 2.1.2. Nutrient and Chlorophyll Climatology from In Situ Measurements

[12] We gathered historical in situ nitrate, ammonium, and chlorophyll observations in the New England shelf region from the World Ocean Database (http://www.nodc.noaa.gov/) and other sources. This totaled 2827 nitrate, 1453 ammonium, and 1852 chlorophyll profiles and 3400 surface chlorophyll observations (see the inset in Figure 1 for locations of all observations). We averaged these data in the along-shelf direction (in the same depth-binned manner as previously described) to produce seasonal cross-shelf nutrient (the sum of nitrate and ammonium) and chlorophyll climatologies (Figure 5).

[13] For comparing the in situ and satellite climatologies of chlorophyll, we first vertically averaged the in situ chlorophyll profiles with an optical weighting function to mimic the satellite

measurement; the results are then averaged in the along-shelf direction to form a cross-shelf distribution of chlorophyll concentration (blue lines in Figure 4). The vertical weighting function takes into consideration light attenuation due to water and chlorophyll absorption in both downward (incoming) and upward (reflected) transmission [*Smith*, 1981]:

$$g(z) = \exp\left(2k_z z + 2k_{Chl}\int_z^0 Chl(z')dz'\right) \quad (1)$$

[14] Here, $k_z = 0.04 \, \text{m}^{-1}$ is the light attenuation coefficient of sea water [*Kirk*, 1994], $k_{Chl}$ is the light attenuation coefficient of chlorophyll, $Chl$ is chlorophyll concentration, and $z$ is water depth (positive upward) with the sea surface located at $z = 0$. Tests suggest that the inferred chlorophyll concentration is not particularly sensitive to the value of $k_{Chl}$, and $0.0316 \, \text{m}^2 \, (\text{mg Chl})^{-1}$ is used here. The 95% confidence intervals (blue dashed lines in Figure 4) of the averaged chlorophyll concentration are also computed, assuming profiles more than 40 km apart in the along-shelf direction (~0.5° longitude) or 10 km apart in the cross-shelf direction (~0.1° latitude) or 3 days apart are independent.

### 2.1.3. Climatology of Surface and Bottom Mixed Layer Depths

[15] Vertical mixing is crucial for ecosystem dynamics in the shelfbreak region, but the 2-D physical model in *Zhang et al.* [2011] does not accurately depict the effective mean vertical mixing in the surface and bottom boundary layers
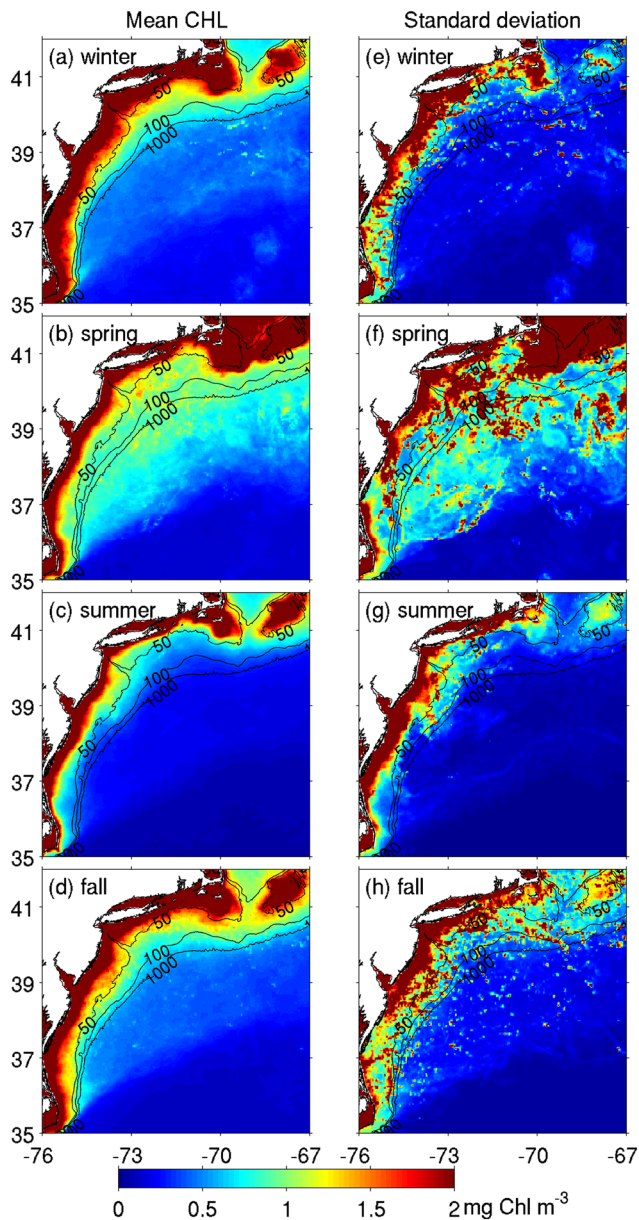
**Figure 3.** Seasonal climatology (left column) and standard deviation (right column) of surface chlorophyll in the MAB area compiled from 8 years of MODIS observations.

mean vertical diffusivity may be disproportionately influenced by episodic storm events. Therefore, the diffusivity profile induced by seasonal mean wind forcing differs from the time-averaged diffusivity profile of a model forced by time-dependent winds. Last, the model does not include tides, which affect the strength of the near-bottom turbulence through oscillatory bottom flows, and therefore the intensity of near-bottom turbulence mixing in the model is underestimated.

[16] Because of these deficiencies, the surface and bottom mixed layers generated in the 2-D physical model are much thinner than the mean MLDs. For instance, the surface MLD at the shelfbreak given by the model turbulence closure in the winter simulation using seasonal mean winds is about 15 m, much thinner than the observed mean surface MLD of about 50 m (see below). Misrepresentation of the mean MLDs and vertical diffusivity in the model does not affect the modeled mean circulation since the model temperature and salinity fields are nudged toward the climatology. However, it will affect the balance of biological tracers and the associated biological production in the shelfbreak region (section 3.5). One way to avoid that is to specify climatological mean profiles of vertical diffusivity for each season in the model. Unfortunately, the seasonal mean profiles of vertical diffusivity in the region are difficult to quantify due to the lack of long-term direct measurements of vertical mixing. Synoptic observations of vertical diffusivity in the area [*Ledwell et al.*, 2004; *MacKinnon and Gregg*, 2003; 2005; *Rehmann and Duda*, 2000] mostly focus on mixing in the middle and lower water column, to which local biological productivity is less sensitive (see below). Moreover, because of the nonlinear nature of vertical mixing, it is challenging to estimate seasonal mean profiles of vertical diffusivity from synoptic observations. Here, we take an indirect approach and estimate climatological mean profiles of vertical diffusivity through computing climatological surface and bottom MLDs from historical in situ temperature observations. Vertical diffusivity in the surface and bottom mixed layers are specified to generate seasonal mean profiles of vertical diffusivity, which are then used in the corresponding seasonal simulations.

[17] Historical temperature profiles (62,478 in total) in the New England shelf region [*Fleming and Wilkin*, 2010] are used to compute the seasonal mean MLDs. Surface MLD is estimated for each profile using a threshold method with a 0.5°C temperature difference criterion from the reference level of 2 m below the surface. Bottom MLD is estimated similarly with a 0.25°C temperature difference criterion from the deepest observation in each profile. The estimated MLDs are bin averaged in the along-shelf direction to generate the seasonal surface and bottom MLD climatology (solid lines in Figure 6) along with the corresponding 95% confidence intervals (dashed lines in Figure 6). In computing the confidence intervals, profiles more than 40 km apart in the along-shelf direction or 10 km apart in the cross-shelf direction or 3 days apart are assumed independent. Notice that the bottom MLD is not computed for the area offshore of the shelfbreak because near-bottom stratification there is dramatically different from that on the shelf. Since near-bottom vertical diffusion in the deep area does not affect the near-surface mixing of biological tracers, we simply extend the bottom MLD at the shelfbreak offshore.

for several reasons. First, the 2-D temperature and salinity climatology to which the model is nudged (section 2.2) does not provide the correct surface or bottom mixed layer depths (MLDs). Because averaging temperature and salinity profiles tends to spread stratification over the whole water column (see Figure 3 in *Zhang et al.* [2011]), the MLD computed from climatology is usually thinner than the average of MLDs computed from individual profiles using the same criteria. As vertical diffusivity is generally high in the surface and bottom mixed layers and low in the interior, misrepresentation of the MLDs in the density field hinders the model from proper representation of the effective mean vertical diffusivity. Second, the model is forced by seasonal mean winds. The effect of winds on vertical mixing in the shelfbreak area is nonlinear, and the effective
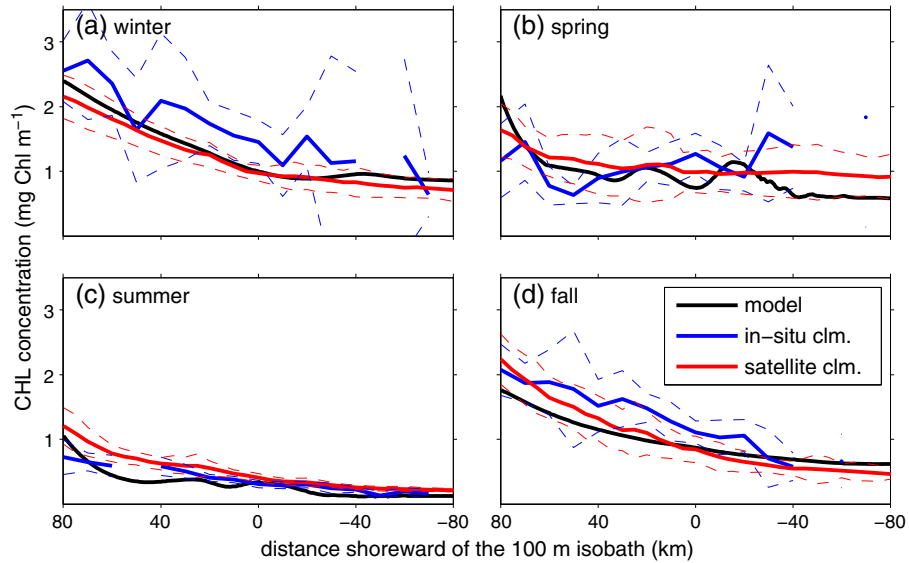
**Figure 4.** Cross-shelf distribution of chlorophyll concentration calculated from the seasonal satellite (red solid lines) and in situ (blue solid lines) climatologies, and model control simulations (black lines). The dashed lines outline the 95% confidence intervals of the averaged distribution of satellite (red) and in situ (blue) chlorophyll.
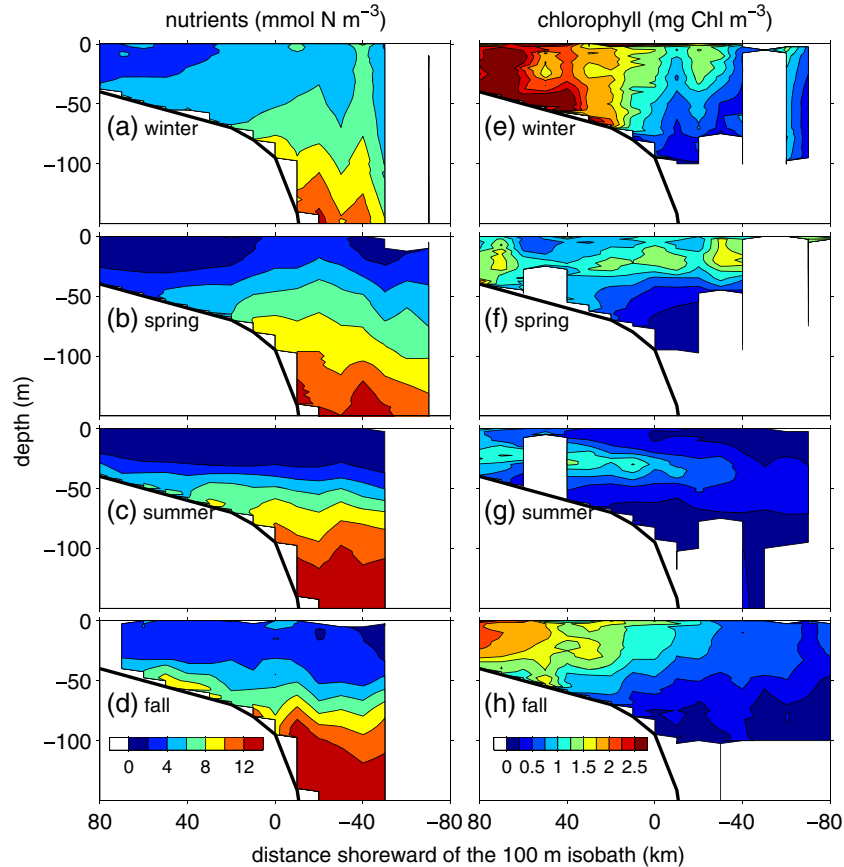


**Figure 5.** Cross-shelf distribution of along-shelf and seasonally averaged nutrients (nitrate plus ammonium; left column) and chlorophyll (right column) computed from historical in situ observations in the New England shelf area (Figure 1).
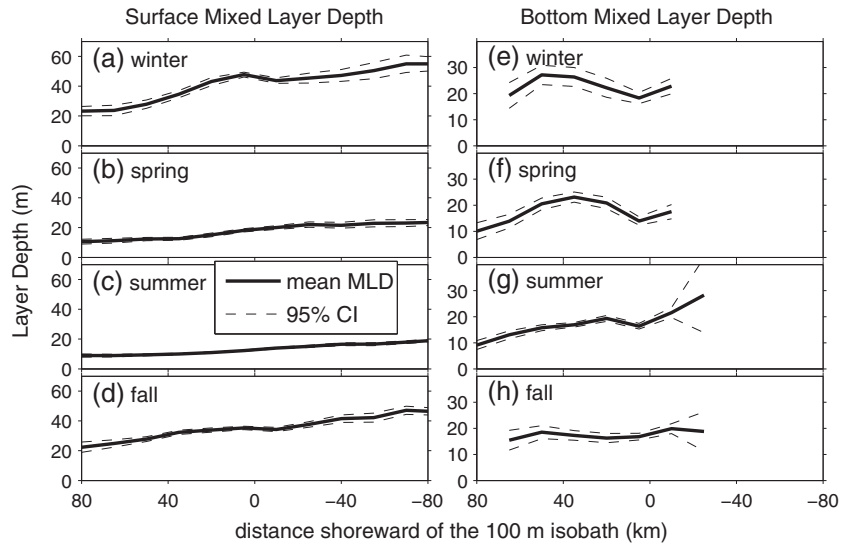
**Figure 6.** Observed cross-shelf distribution of the along-shelf and seasonally averaged surface (left column) and bottom (right column) mixed layer depth (solid lines) and the corresponding 95% confidence intervals (dashed lines).

[18] Based on the climatological cross-shelf distributions of MLDs, we compiled a field of effective mean vertical diffusivity for each season. Vertical diffusivity within the surface and bottom mixed layers are chosen to be $6 \times 10^{-3}$ and $2 \times 10^{-3} \, \mathrm{m^2 \, s^{-1}}$, respectively. The surface value is about half of the value given by the model turbulence closure in the thin surface mixed layer. In the interior (below the surface mixed layer and above the bottom mixed layer), the prescribed diffusivity reverts to that computed in the model turbulence closure. The vertical diffusivity profiles at the shelfbreak computed by the model turbulence closure scheme and those compiled based on the climatological MLDs are compared in Figure 7.

## 2.2. The Physical Model

[19] The physical model used herein is the same as that in *Zhang et al.* [2011], so only a brief description of the model setup is provided here. The model is based on the Regional Ocean Modeling System (ROMS) [*Shchepetkin and McWilliams*, 2008] and covers a cross-shelf area that is very narrow (~3 km) in the along-shelf direction. The model domain is oriented such that the positive $x$ direction is along-shelf toward the east (upstream) and the positive $y$ direction is toward the north (onshore). The cross-shelf span of the model domain is 290 km, including 140 km onshore and 150 km offshore of the 100 m isobath. The cross-shelf bathymetry is the along-shelf average of the New England shelf area with a cutoff at 1000 m depth (Figure 8 inset). The along- and cross-shelf resolutions are 600 and 500 m, respectively. The model has 60 stretched vertical layers with higher resolution near the surface and bottom to resolve the boundary layers. The onshore (northern) boundary is a solid wall, and the offshore (southern) boundary is open with *Chapman* [1985] and *Flather* [1976] conditions for sea level and barotropic velocity, respectively. An Orlanski-type radiation condition [*Orlanski*, 1976] is specified for momentum and tracers. Periodic boundary conditions are applied in the along-shelf direction (east-west) assuming

no along-shelf variation of temperature, salinity, and velocity. Quadratic bottom drag with a drag coefficient of 0.012 is used. The general length scale (GLS) method *k-kl* type vertical mixing scheme [*Umlauf and Burchard*, 2003; *Warner et al.*, 2005] is used to compute vertical diffusivity in the interior and, as previously described, vertical diffusivity in the surface and bottom mixed layers is prescribed (Figure 7b). Physical variables are initialized with the steady state solutions of *Zhang et al.*
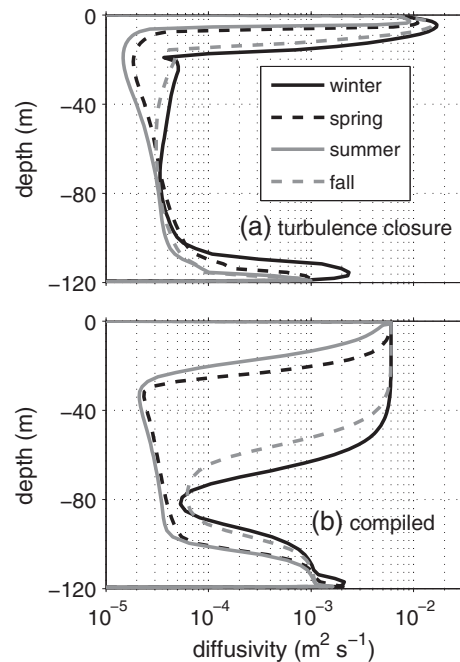


**Figure 7.** Profiles of vertical diffusivity at the shelfbreak (a) computed by the model turbulence closure using seasonal mean wind forcing and (b) compiled based on seasonal mean surface and bottom mixed layer depths.
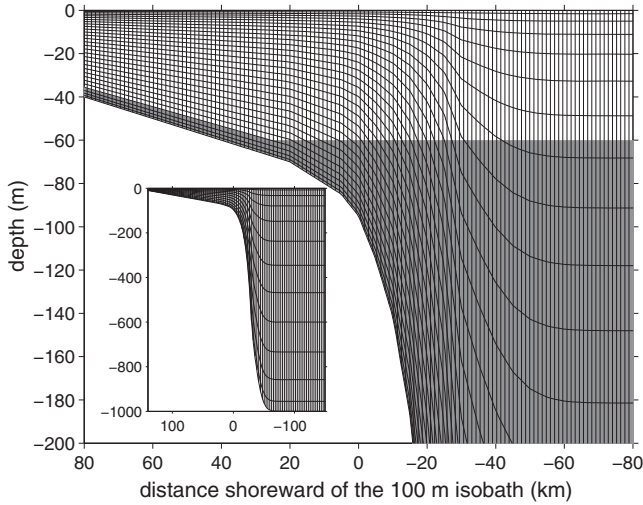
**Figure 8.** Cross-shelf topography and model vertical grid. For clarity, plotted grids have been decimated, and each plotted grid cell in the main figure and in the inset consists of $2 \times 2$ and $5 \times 5$ model grids, respectively. The gray area denotes the region where the model nutrient concentration is nudged toward the initial concentration.

[2011], and the simulations are forced by the seasonal mean winds. Model temperature and salinity are nudged toward the seasonal cross-shelf 2-D climatology that is based on a regional 3-D monthly climatology [*Fleming and Wilkin*, 2010].

## 2.3. The Biological Model

[20] The biological simulations are based on a four-component planktonic ecosystem model similar to the one used in *Powell et al.* [2006]. The biological state variables are dissolved inorganic nutrients ($N$), non-living particulates (Detritus: $D$), phytoplankton ($P$), and herbivorous zooplankton ($Z$). They are all in the nitrogen-based unit of mmol N m$^{-3}$. The governing equations are

$$\frac{\partial N}{\partial t} + \mathbf{u} \cdot \nabla N = \delta D + (1-\gamma)GZ - UP + h\frac{N_0 - N}{\tau} \quad (2)$$
$$+ \frac{\partial}{\partial z}\left(k_v \frac{\partial N}{\partial z}\right)$$

$$\frac{\partial P}{\partial t} + \mathbf{u} \cdot \nabla P = UP\text{-}GZ\text{-}\sigma_d P + \frac{\partial}{\partial z}\left(k_v \frac{\partial P}{\partial z}\right) \quad (3)$$

$$\frac{\partial Z}{\partial t} + \mathbf{u} \cdot \nabla Z = \gamma GZ - \zeta_d Z^2 + \frac{\partial}{\partial z}\left(k_v \frac{\partial Z}{\partial z}\right) \quad (4)$$

$$\frac{\partial D}{\partial t} + \mathbf{u} \cdot \nabla D = \sigma_d P + \zeta_d Z^2 - \delta D + w_d \frac{\partial D}{\partial z} + \frac{\partial}{\partial z}\left(k_v \frac{\partial D}{\partial z}\right) \quad (5)$$

where $\mathbf{u}$ is velocity vector, $\nabla$ is gradient operator ($\partial/\partial x$, $\partial/\partial y$, $\partial/\partial z$), $N_0$ is the initial condition for nutrients (based on climatology; see below), $\tau$ is nudging time scale, and $k_v$ is vertical diffusivity. The first terms in the left-hand side of equations (2)–(5) are local changes of the biological variables with time, and the last terms in the left- and right-hand sides stand for advection and vertical diffusion, respectively. Equation (2) contains a nudging term, $h(N_0 - N)/\tau$, that we will discuss later in this section. The only state variable with a sinking rate is detritus, and that process is represented as $w_d$

($\partial D/\partial z$). The rest of the terms depict the interaction between the biological variables.

[21] In order to compare with chlorophyll observations, we assume a constant ratio of nitrogen to chlorophyll in phytoplankton, with carbon as an intermediate step (C:N = 6.6 and C:Chl = 50 g C (g Chl)$^{-1}$). In reality, variations in both ratios can occur in phytoplankton [e.g., *Cullen*, 1982], but how they vary in the study area on seasonal time scales is unknown. We therefore assume these ratios are constant to reduce the number of unconstrained parameters in the model.

[22] The phytoplankton growth rate ($U$), zooplankton grazing rate ($G$), and irradiance profile ($I(z)$) are formulated as

$$U = \frac{V_m N}{k_N + N} \frac{\alpha I}{\sqrt{V_m^2 + \alpha^2 I^2}} e^{C_p(T-T_0)} \quad (6)$$

$$G = R_m e^{C_z(T-T_0)}\left(1 - e^{-\Lambda P}\right) \quad (7)$$

$$I(z) = \beta I_0 \exp\left(k_z z + k_p \int_z^0 P\left(z'\right) dz'\right) \quad (8)$$

[23] Here, $T$ is temperature and $I_0$ is surface irradiance. All other biological parameters in equations (2)–(8) are listed in Table 1.

[24] Equations (2)–(8) differ from the model of *Powell et al.* [2006] in three important ways. First, the phytoplankton growth (equation (6)) and zooplankton grazing (equation (7)) rates are temperature dependent with $Q_{10}^p = e^{10C_p}$ and $Q_{10}^p = e^{10C_z}$, respectively. Temperature exerts profound influences on the growth of both phytoplankton and zooplankton [*Brush et al.*, 2002; *Durbin and Durbin*, 1996; *Eppley*, 1972; *Huntley and Lopez*, 1992; *Mousseau et al.*, 1996; *Rose and Caron*, 2007]. Because the annual temperature range on the New England shelf is very large (~20°C; Figures 2a–2d), these $Q_{10}$ terms are necessary to account for seasonal variations in maximal growth rates. Note that the temperature influences are implemented in equations (6) and (7) using the same reference temperature $T_0$. This avoids introduction of a redundant unknown parameter in the model, insofar as both the rate coefficients ($V_m$ and $R_m$) and temperature dependent coefficients ($C_p$ and $C_z$) are adjustable parameters. Therefore, using the same $T_0$ in equations (6) and (7) does not reduce the degrees of freedom in the temperature dependence of the simulated autotrophic and heterotrophic processes.

[25] The second departure from the *Powell et al.* [2006] model is that zooplankton mortality is quadratic instead of linear. The quadratic form, first introduced by *Steele and Henderson* [1981], is an effective way to parameterize the predation of zooplankton by higher trophic levels [*Edwards and Brindley*, 1996; *Fasham*, 1995]. We found this formulation to be necessary for accurate simulation of the cross-shelf gradient in phytoplankton—without it the zooplankton population could always grow large enough to graze the phytoplankton population down to a quasi-uniform cross-shelf distribution. The quadratic form also helped eliminate predator-prey oscillations present in the model with linear mortality.

[26] The third difference is the nudging term in equation (2). It restores the nutrient fields toward the initial conditions ($N_0(z)$, provided by observations) on a time scale ($\tau$) of 1 day. Our primary purpose is to simulate the biological response to the upwelling at the shelfbreak, and this nudging

**Table 1.** Biological Parameters Used in This Study and Range of Published Parameter Values

| Parameter Name | Symbol | Value | Unit | Range |
|---|---|---|---|---|
| Active portion of shortwave radiation | $\beta$ | 0.43 | - | 0.43[1]–0.5[2] |
| Reference temperature | $T_0$ | 8 | °C | - |
| Temperature coef. of phytoplankton growth | $C_P$ | 0.06 | °C$^{-1}$ | 0.06[3]–0.0633[4] |
| Temperature coef. of zooplankton growth | $C_z$ | 0.12 | °C$^{-1}$ | 0.0359[5]–0.13[3] |
| Chlorophyll attenuation coefficient | $k_p$ | 0.05 | m$^2$ mmol N$^{-1}$ | 0.0095[6]–0.076[2,7] |
| Initial slope of P-I curve | $\alpha$ | 0.009 | m$^2$ (W day)$^{-1}$ | 0.0016–0.031[1,8] |
| Nutrient uptake rate coef. | $V_m$ | 1.5 | day$^{-1}$ | 0.62–3.0[1] |
| Nutrient uptake half saturation | $k_N$ | 0.2 | mmol N m$^{-3}$ | 0.007–1.5[1] |
| Phytoplankton mortality rate | $\sigma_d$ | 0.06 | day$^{-1}$ | 0.05-0.2[1] |
| Zooplankton growth rate coef. | $R_m$ | 0.33 | day$^{-1}$ | 0.01[9]–1.0[1] |
| Ivlev constant | $\Lambda$ | 1.5 | m$^3$ mmol N$^{-1}$ | 0.06[5]–1.4[10] |
| Zooplankton assimilation efficiency | $\gamma$ | 0.8 | - | 0.25[11]–0.75[1] |
| Quadratic zooplankton mortality rate | $\zeta_d$ | 3.0 | m$^3$ (mmol N day)$^{-1}$ | 0.05[12]–2.0[13] |
| Remineralization rate | $\delta$ | 0.1 | day$^{-1}$ | 0.01–0.25[1] |
| Detritus sinking rate | $w_d$ | 8 | m day$^{-1}$ | 0.009–25[1] |

[1]*Fennel el al.* [2006].
[2]*Walsh et al.* [2005].
[3]*Rose and Caron* [2007].
[4]*Eppley* [1972].
[5]*Hirst and Bunker* [2003].
[6]*Powell et al.* [2006].
[7]Note that the unit has been converted from m$^2$ (mg Chl)$^{-1}$ in *Walsh et al.* [2005] to m$^2$ mmol N$^{-1}$.
[8]Note that the unit has been converted from mol C gChl$^{-1}$ m$^2$ (W day)$^{-1}$ in *Fennel et al.* [2006] to m$^2$ (W day)$^{-1}$.
[9]*Riley* [1942]
[10]*Shigemitsu et al.* [2012]
[11]*McGillicuddy et al.* [1995].
[12]*Fennel et al.* [2001].
[13]*Edwards and Brindley* [1996].

assures that the nutrient concentration in the upwelled water is realistic. Nudging operates in an area depicted by $h$: the bottom 1/8 of the water column shoreward of the 65 m isobath and below 60 m offshore (shaded area in Figure 8). $h$ is 1 in the nudging area and 0 everywhere else. The model nutrient initial conditions are horizontally uniform, increasing linearly with depth to a maximum of 13 mmol N m$^{-3}$. The downward increasing trend in each season was obtained from a linear fit to a cross-shelf-averaged profile of the in situ nutrient climatology near the shelfbreak (Figures 5a–5d). This nudging is necessitated by the fact that some of the key 3-D processes that maintain the cross-shelf distribution of nutrients are not included in our 2-D model, namely along-shelf advection from upstream and cross-shelf eddy fluxes. The near-bottom nudging of $N$ on the shelf also helps to compensate for the neglect of bottom organic matter remineralization, which is thought to be an important source of nutrients in the MAB region [*Fennel et al.*, 2006]. We emphasize that the restoration below 60 m does not provide nutrients directly to the euphotic zone (top 50 m) and only influences phytoplankton growth indirectly through upwelling or mixing. Test simulations with nudging cutoff depths of 50 and 80 m show little difference in model results.

[27] Four diagnostic simulations are conducted, with one for each season. The initial conditions for $P$, $Z$, and $D$ are spatially uniform with $P_0 = 2$ mmol N m$^{-3}$, $Z_0 = 0.1$ mmol N m$^{-3}$, and $D_0 = 1$ mmol N m$^{-3}$, respectively. The seasonally averaged surface irradiances, $I_0$, calculated from NCEP 1949–2011 reanalysis in the New England shelf area, are 111, 230, 218, and 92 W m$^{-2}$ for winter, spring, summer, and fall seasons, respectively. Boundary conditions for the biological variables are Orlanski-type radiation conditions on the offshore (southern) boundary and periodic conditions in the along-shelf direction. Each simulation is run for

100 days, during which the initial transients equilibrate and the model achieves a quasi-steady state representing the mean biological response to the mean physical conditions of that season. Results reported below are drawn from the quasi-steady state solutions.

## 3. Results

### 3.1. Seasonal Climatology of Nutrients and Chlorophyll

[28] Satellite-derived mean surface chlorophyll distributions in all seasons (Figure 3) share the general pattern of high concentration near the coast and gradually decreasing concentrations offshore. Chlorophyll concentrations near the coast are higher in fall and winter relative to the other two seasons, and concentration in the slope sea is the highest in spring. Meanwhile, standard deviations of chlorophyll concentration in all seasons are on the same order as the seasonal means, suggesting that surface chlorophyll in the MAB area has strong temporal variability on shorter time scales. Along-shelf averages (red lines in Figure 4) reveal the decrease in chlorophyll from the shelf to the slope sea is relatively smooth and monotonic in all seasons.

[29] A notable aspect of the seasonal climatology is the absence of a local maximum of chlorophyll concentration at the shelfbreak. This is consistent with the climatologies of *Yoder et al.* [2002] and *O'Reilly and Zetlin* [1998] but is in contrast to the enhancement along the shelfbreak observed in synoptic satellite images during springtime [*Ryan et al.*, 1999a]. At least two factors could cause the apparent difference: (i) the magnitude of the enhancement is not sufficient to rise above the variability in the data, and (ii) the mechanism(s) responsible for generating the synoptic enhancement is (are) not as effective on a seasonal time scale. We will return to this issue in section 4.2.

[30] Near-surface chlorophyll distributions in the in situ climatology (Figures 5e–5h) resemble the satellite climatology in terms of the cross-shelf variability. The in situ data show subsurface chlorophyll maxima across the shelfbreak in spring and summer. That pattern is particularly distinct in summer, with the subsurface concentration at the shelfbreak ($\sim$1.25 mg Chl m$^{-3}$) almost an order of magnitude higher than the surface ($<$0.25 mg Chl m$^{-3}$). Because few in situ chlorophyll observations are available offshore of the shelfbreak during spring, the in situ climatology is unable to resolve the vertical distribution of the springtime chlorophyll in much of the slope sea.

[31] Extracting a satellite view of the in situ chlorophyll concentration via equation (1) produces a cross-shelf distribution that generally matches the along-shelf averaged satellite climatology (Figure 4). However, there are a few exceptions. First, the chlorophyll concentration in the in situ climatology is somewhat higher than that in the satellite-derived climatology in winter when fewer profiles are available. Correspondingly, the 95% confidence interval of the in situ climatology is much wider and overlaps the values from the satellite-derived climatology. Second, the summertime concentration in the in situ climatology is slightly lower than that in the satellite-derived climatology at the coast. A possible explanation of this discrepancy is contamination of the satellite-derived chlorophyll by colored dissolved organic matter [*Siegel et al.*, 2005]. Nevertheless, the general agreement between the two types of observations suggests that the seasonal pattern of chlorophyll distribution is robust.

[32] Nutrient distributions in the in situ climatology in all seasons (Figures 5a–5d) have a general trend of increasing with depth. At 100 m, the concentration is about 10–12 mmol N m$^{-3}$. The surface concentration in winter and fall is 2–4 mmol N m$^{-3}$, reflecting an excess of surface nutrients owing to light limitation. The wintertime surface concentration increases gradually offshore, from 2 mmol N m$^{-3}$ on the mid-shelf to about 4 mmol N m$^{-3}$ at the shelfbreak. The lower concentration of nutrients inshore during winter is consistent with an inner-shelf winter bloom documented in prior studies [*Xu et al.*, 2011; *Yoder et al.*, 2002]. The surface nutrient level is low ($<$2 mmol N m$^{-3}$) in spring and almost completely depleted in summer as a consequence of the high biological utilization during those seasons. The nutrient field is comprised primarily of nitrate. Ammonium concentration is negligible everywhere except near-bottom on the shelf where it reaches about 2–3 mmol m$^{-3}$ (not shown).

## 3.2. Fitting the Model to the Observations

[33] We sought a solution to the model equations that fit the observed seasonal variation in cross-shore distribution of chlorophyll from satellite and in situ climatologies, as well as nitrate in the upper ocean where it was free to evolve in the model (Figures 4 and 5). This was accomplished by running hundreds of trial simulations in which model parameters were varied systematically. Although more sophisticated approaches to parameter estimation are possible [e.g., *Friedrichs et al.*, 2007], we did not utilize such methods in our study. Nevertheless, we were able to ascertain a parameter set for which the model is generally consistent with the observations (Table 1). For the most part, the parameter values fall within the ranges used in prior modeling studies. It is certainly possible that equal or better fits to the data could be achieved

with different parameter values, but an exhaustive search of parameter space is not practical for this problem.

## 3.3. Modeled Seasonal Distribution of Biological Variables

[34] Because of the nudging, the model nutrient concentration below 60 m does not deviate far from its initial condition and the relatively high concentration near the bottom over the shelf is preserved in all seasons (Figures 9a–9d). In the upper 60 m, the modeled nutrient concentrations resemble those in the in situ climatology in winter and summer seasons. However, the modeled near-surface nutrient concentration offshore of the shelfbreak is about 2 mmol N m$^{-3}$ lower than the climatology during spring and 2–4 mmol N m$^{-3}$ higher than the climatology during the fall.

[35] Simulated chlorophyll fields (Figures 9e–9h) capture the general patterns of the observed cross-shelf (Figure 4) and vertical (Figures 5e–5h) distributions. Specifically, (1) in all seasons, chlorophyll decreases from inshore to offshore; (2) in winter and fall, chlorophyll decreases with depth and is near zero below 100 m; (3) in spring and summer there are subsurface maxima; and (4) there is strong seasonal variation on the shelf, with highest concentrations in the winter and lowest in the summer. There are also discrepancies between the simulated and observed distributions. For instance, modeled fall/winter chlorophyll concentration on the shelf (Figures 9e and 9h) is lower than that in the climatology, although the cross-shelf distributions fall within the error bounds of the satellite and in situ climatologies (Figures 4a and 4d). In addition, the springtime subsurface maximum is less pronounced in the model than it is in the observations, and the summertime subsurface maximum is thinner in the model than in the data.

[36] One particularly noteworthy feature of the modeled chlorophyll in spring is the relatively high concentration ($\sim$1 mg Chl m$^{-3}$) in the upper 30 m about 20 km offshore of the shelfbreak (100 m isobath) (Figure 9f). This peak of surface chlorophyll concentration results from the shelfbreak upwelling (Figure 2f) that brings nutrient-rich slope water across the nutricline and into the euphotic zone (see section 3.3 for more discussion). Despite the low vertical velocity ($\sim$0.15 m d$^{-1}$ at 30 m depth; Figure 2f), the upwelling is able to transport nutrients into the euphotic zone, and mixing in the upper ocean (Figure 7b) redistributes the upwelled nutrients over the entire surface mixed layer and enhances the local primary production. However, this peak in chlorophyll concentration near the shelfbreak is not significant compared to the 95% confidence intervals of the climatologies (Figure 4b).

[37] Modeled zooplankton concentrations (Figures 10a–10d) show strong seasonal variation with the lowest concentration in winter and highest in summer. The zooplankton concentrations in winter, spring, and fall are generally vertically uniform in the surface mixed layer and decrease rapidly at greater depth. In contrast, a distinct subsurface maximum occurs across most of the shelf during summer. Modeled zooplankton concentrations exhibit maxima near the shelfbreak during spring and summer. The elevated concentration at the shelfbreak in the surface mixed layer is about the same in the two seasons ($\sim$0.07 mmol N m$^{-3}$), but the summer distribution has a shelfbreak subsurface peak concentration that is considerably higher ($>$0.12 mmol N m$^{-3}$).
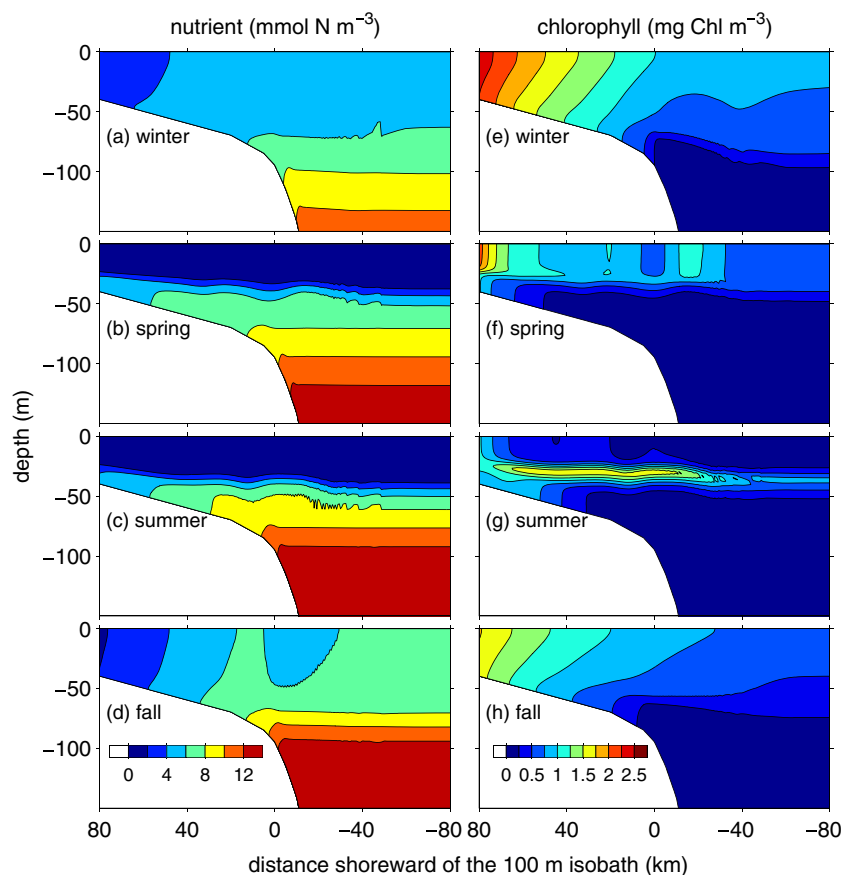
**Figure 9.** Cross-shelf sections of the modeled nutrient (left column) and chlorophyll (right column) concentrations in different seasons. Notice that the phytoplankton concentration has been converted from nitrogen-based units to chlorophyll-based units.

[38] Given the importance of zooplankton grazing in our model solutions, it is of interest to compare the predicted rates with observations. The ingestion rates, $\gamma G$, at the shelf-break in the model, steady state solutions are 0.14–0.2, 0.18–0.24, 0.24–0.48, and 0.24–0.32 day$^{-1}$ in winter, spring, summer, and fall, respectively. *Smith and Lane* [1988] estimated springtime ingestion rates of several herbivorous copepods in the study area of 31–80% bodily C day$^{-1}$. However, there is ample evidence of a wide range of grazing rates in other areas such as the Chesapeake Bay (0.08–2.80 bodily C day$^{-1}$) [*White and Roman*, 1992], the North Sea (0.35–0.56 bodily C day$^{-1}$) [*Gamble*, 1978] as well as in the laboratory (0.28–4.81 bodily C day$^{-1}$) [*Paffenhöfer*, 1971]. Given the strong seasonal and interannual variability of zooplankton community composition and abundance that have been observed in the MAB shelfbreak area [*Flagg et al.*, 1994; *Judkins et al.*, 1980], the fact that the simulated rates are bracketed by observational estimates suggests that the modeled zooplankton dynamics is not unrealistic. Note that the modeled zooplankton includes microzooplankton, for which there is a paucity of measurements of in the study area.

[39] Modeled detritus concentrations (Figures 10e–10h) show seasonal variation similar to that of phytoplankton: higher in winter and fall, and lower in spring and summer. Similar to the cross-shelf variation of phytoplankton, detritus concentrations are generally higher inshore than offshore. Available

particle flux measurements [*Biscaye and Anderson*, 1994] are generally consistent with this cross-shore trend in the simulated distribution of detritus. Upper ocean detritus concentration in the model increases with depth during all seasons, and peak values (0.2–0.36 mmol N m$^{-3}$) occur near the bottom over the shelf and at the base of the surface mixed layers offshore. The downward decrease in concentration below the peaks reflects loss due to remineralization. Detritus concentrations in spring and summer also show shelfbreak subsurface maxima ($\sim$0.2 mmol N m$^{-3}$), resulting from the relatively high biological production at the shelfbreak in the model. The enhanced biological productivity simulated at the shelf break may potentially contribute to the observed increase in particle fluxes near the bottom on the upper slope [*Biscaye and Anderson*, 1994], although some offshore transport in the bottom boundary layer would be required.

### 3.4. Nutrient and Chlorophyll Budgets

[40] To understand the dynamics of nutrients and phytoplankton (chlorophyll) in the model, we vertically integrated the terms in equations (2) and (3) over the upper 50 m (Figure 11). The temporal derivative terms are zero in steady state and therefore neglected in Figure 11. Cross-shelf sections of the phytoplankton growth term in all seasons (Figures 12a–12d) show that phytoplankton growth takes place predominantly in the upper 50 m. Therefore, the vertical integration corresponds approximately to the euphotic zone.
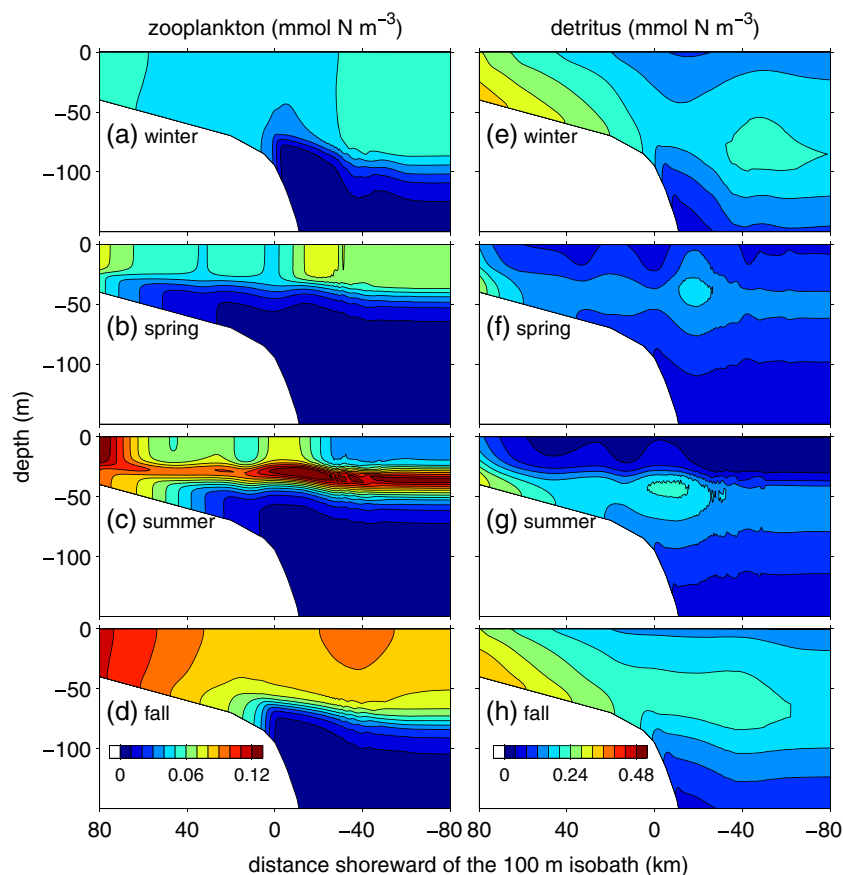
**Figure 10.** Cross-shelf sections of the modeled zooplankton (left column) and detritus (right column) concentrations in different seasons.

[41] Phytoplankton uptake in the surface layer is a major sink of nutrients in all seasons (Figures 11a–11d). In winter and fall when vertical diffusivity is high over the entire layer of the upper 50 m (Figure 7b), vertical diffusion is a major source of nutrients to the euphotic zone. Diffusion is less important in spring and summer when contributions from other terms, such as advection and remineralization, become comparable. In spring and summer, the advection term is the largest source at the shelfbreak, reflecting the role of upwelling in providing nutrients to the surface layer in those two seasons. The supply of nutrients by the upwelling is dominant at the shelfbreak in summer as the advection term is twice as large as the next leading term, remineralization. The role of the upwelling is reduced in spring as the advection term is only slightly higher than the remineralization term at the shelfbreak. In the 0–50 m nutrient balances, the nudging term is zero everywhere except the inshore area where the near-bottom nudging zone is shallower than 50 m (Figure 8).

[42] In all seasons, phytoplankton dynamics are dominated by the balance between growth and mortality (Figures 11e–11h). Phytoplankton growth is concentrated near the surface in winter and fall when light is limiting, whereas productivity peaks deeper in the euphotic zone in spring and summer when nutrients are the limiting factor (Figures 12a–12d). Zooplankton grazing constitutes an important loss in all seasons, but its role in the phytoplankton balance becomes more important in summer and fall when the water column is relatively warm. This can also been seen in

the cross-shelf section of the zooplankton grazing term (Figures 12e–12h). Patterns of zooplankton grazing are similar to those of zooplankton concentrations (Figures 10a–10d) with particularly high grazing rates in summer and fall. Peak summertime zooplankton grazing coincides with the subsurface peak in phytoplankton growth at the shelfbreak (Figures 12c and 12g). The springtime grazing rate has a minor peak at the shelfbreak in the surface mixed layer. These shelfbreak peaks in zooplankton grazing rate in spring and summer are evident in the vertically integrated grazing term (Figures 11f–11g). Vertical diffusion constitutes a significant sink of phytoplankton in winter and fall when strong vertical mixing redistributes some of the phytoplankton produced near the surface to depths below 50 m (Figures 11e–11h).

## 3.5. Sensitivity of the Chlorophyll Distribution to Model Parameters

[43] We investigated sensitivities of the model results to the biological parameters in Table 1 by comparing the solutions of the baseline seasonal simulations described above and additional runs in which each parameter was perturbed ±50% (Appendix A). The comparisons show that results of the biological model are sensitive to several of the biological parameters, including the reference temperature, temperature coefficients of phytoplankton and zooplankton growth, the initial slope of the P-I curve, the chlorophyll attenuation coefficient, the phytoplankton mortality rate, and the zooplankton growth and mortality coefficients. These results highlight the
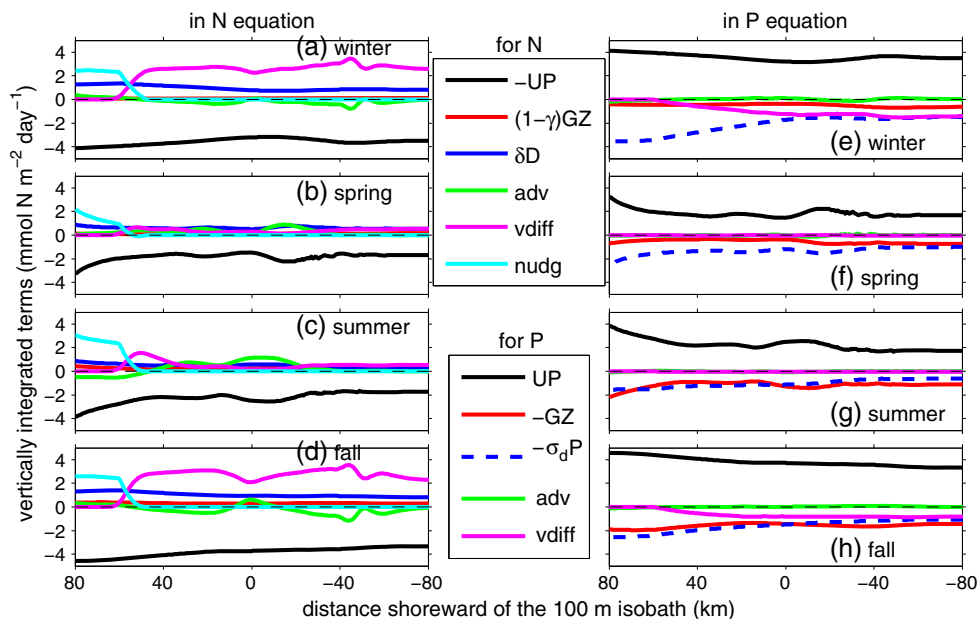
**Figure 11.** Vertically integrated terms in the nutrient (equation (2); left column) and phytoplankton (equation (3); right column) budgets over the upper 50 m in different seasons. Names of the biological terms in the legends are consistent with the notation in equations (2) and (3): $\pm UP$ stands for phytoplankton growth, $(1-\gamma)GZ$ zooplankton excretion/egestion, $\delta D$ detritus remineralization, $-GZ$ zooplankton grazing, and $-\sigma_d P$ phytoplankton mortality; "adv" stands for the sum of horizontal and vertical advection, "vdiff" vertical diffusion, and "nudg" nutrient nudging.

necessity of the enhancements to the *Powell et al.* [2006] model required to fit the data, namely temperature dependence of phytoplankton growth and zooplankton grazing rates, as well as the addition of a quadratic mortality term in the zooplankton component.

[44] We also conducted sensitivity tests with respect to vertical diffusivity (Appendix B) to examine the influence of mixing on the mean cross-shore distribution of chlorophyll. The tests show that model solutions are sensitive to the prescribed vertical diffusivity in the upper water column, especially to that around the base of the euphotic zone. Results illustrate the importance of vertical mixing in regulating shelfbreak primary production and the necessity of specifying the MLD-based seasonal mean profiles of vertical diffusivity in the model. This highlights the need for better understanding of the effects of local mixing on the shelfbreak ecosystem through systematic measurements of mixing processes.

## 4. Discussion

### 4.1. Shelf-Wide Distributions of Chlorophyll and Zooplankton

[45] The large-scale seasonal variations of chlorophyll present in our climatologies and simulated in our model are consistent with prior studies [*Fennel et al.*, 2006; *Hofmann et al.*, 2011; *O'Reilly and Zetlin*, 1998; *Xu et al.*, 2011; *Yoder et al.*, 2002]. In particular, the highest chlorophyll concentration occurs on the shelf in winter ($>2.5\,\text{mg Chl m}^{-3}$; Figure 5e), which is similar to the wintertime mid-shelf phytoplankton bloom described by *Xu et al.* [2011]. The observed chlorophyll concentrations in the slope sea are the highest in spring (Figures 3 and 4), which is a feature that is not particularly well represented in the model (Figures 4 and 9).

[46] Evaluating the simulated seasonal variations in zooplankton is made difficult by the fact that the modeled zooplankton population includes microzooplankton (with growth rates similar to that of phytoplankton), and existing data are insufficient to specify a reliable cross-shelf distribution. The most extensive zooplankton data sets pertain to larger size fractions sampled with a 333 μm mesh net [*Sherman et al.*, 1998; *Sherman et al.*, 1996b]. Nevertheless, there are some commonalities among the simulated and observed patterns. For example, the simulated zooplankton concentration is highest in summer and lowest in winter (Figures 10a–10d). The wintertime minimum is consistent with results of historical shelf-wide bongo net zooplankton surveys in the area [*Sherman et al.*, 1998]. However, the surveys show shelf-wide mean zooplankton concentrations peak in late spring and early summer (around June) with intermediate concentrations in the fall (see Figure 2c in *Sherman et al.* [1998]). In contrast, our model predicts maxima in the summer and fall. Additional time series data on microzooplankton would be beneficial for constraining the zooplankton component of the model.

[47] Another key aspect of the zooplankton component of the model requiring further study is its temperature dependence. The influence of temperature on zooplankton growth has been observed and quantified in other regions [*Huntley and Lopez*, 1992; *Rose and Caron*, 2007]. How applicable those relationships are on the MAB continental shelf is unknown. We found that having temperature-dependent zooplankton grazing in the model is essential for matching the observed variations in chlorophyll. Specifically, the temperature dependence prescribed in equation (7) allows grazing pressure to be reduced during the light-limited winter bloom period, while still providing for top-down
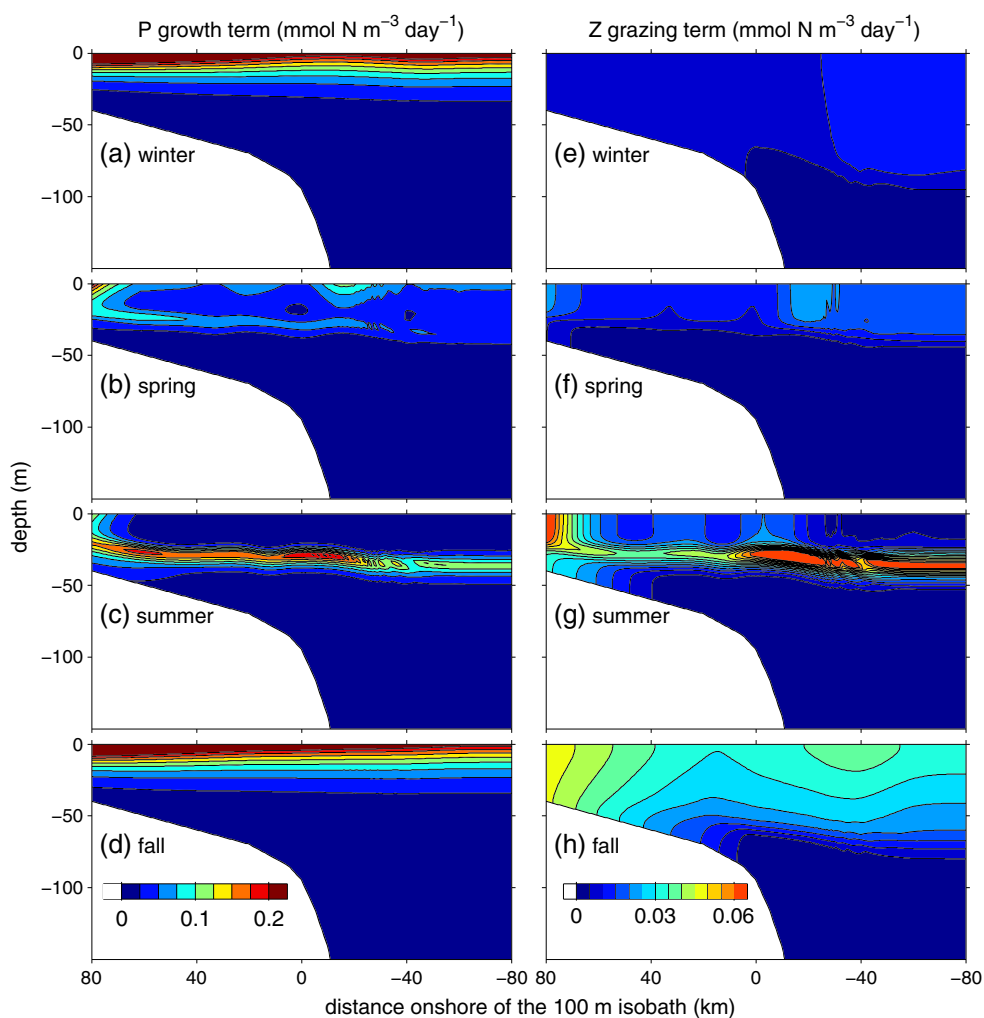
**Figure 12.** Cross-shelf sections of the phytoplankton growth (left column) and zooplankton grazing (right column) terms in different seasons.

control of the phytoplankton population during the time when upwelling at the shelfbreak front enhanced productivity in the spring and summer. The impact of this temperature dependence is particularly evident in the transition between fall and winter solutions: phytoplankton concentration (Figures 9e and 9h), the secondary circulation (Figures 2e and 2h), and the prescribed vertical diffusivity profiles (Figure 7b) are similar, yet the zooplankton concentrations are quite different. The drastic decline in zooplankton concentration from fall to winter is a condition that permits the wintertime bloom of phytoplankton in the model.

### 4.2. Shelfbreak Biological Productivity

[48] Because biological production across the shelfbreak in spring and summer seasons is largely nutrient limited, mean upwelling as portrayed by the 2-D physical model of *Zhang et al.* [2011] brings nutrients from the deep slope sea up into the euphotic zone and stimulates production at the shelfbreak. Satellite and in situ observations over the synoptic scale sometimes show enhanced surface or subsurface chlorophyll concentration at the shelfbreak in spring and summer [*Marra et al.*, 1990; *Ryan et al.*, 1999a]. However, neither our in situ nor satellite climatologies show

significant enhancement of chlorophyll at the shelfbreak in any season (Figures 3b, 3c, 5f, and 5g). One possible reason for the absence of enhanced chlorophyll concentration at the shelfbreak is local consumption of phytoplankton by zooplankton, which would tend to suppress the signal of enhanced shelfbreak productivity in the chlorophyll distribution.

[49] In the model, the persistent shelfbreak upwelling, although weak, enhances local biological productivity in spring and summer (Figures 12b and 12c). However, elevated zooplankton grazing (Figures 12f and 12g) prevents a large buildup of phytoplankton at the shelfbreak. There is a slight enhancement of phytoplankton biomass at the shelfbreak in spring, but its magnitude is within the 95% confidence interval of the climatologies (Figure 4b). This minor peak is a result of stronger upwelling in spring versus summer (Figures 2f and 2g), together with a tendency for weaker grazing because the water is still relatively cold (~8°C). In summer there is no discernible impact of the upwelling on phytoplankton biomass (Figure 4c) because of the weaker upwelling and enhanced grazing due to the warm temperature (14–18°C). In both spring and summer seasons, there are peaks in zooplankton concentration at the shelfbreak (Figures 10b and 10c).

[50] The lack of significant chlorophyll enhancement at the shelfbreak in our climatologies and model simulations is not incompatible with prior studies that document elevated chlorophyll in synoptic observations [e.g., *Marra et al.*, 1990; *Ryan et al.*, 1999a]. From an observational perspective, this simply indicates that the magnitude of the enhancement is not sufficient to rise above the variability, which is large in this region (Figure 3). From a modeling point of view, the fact that climatological mean 2-D simulations with steady forcing show no chlorophyll enhancement at the shelfbreak in no way precludes the presence of such enhancements in circumstances when the forcing is time dependent. Specifically, enhancement of phytoplankton biomass can emerge in response to transient local nutrient input events, when the phytoplankton population becomes temporarily decoupled from the zooplankton population—such as that which can occur in response to upwelling associated with storm events [*Walsh et al.*, 1978] or meandering of the shelfbreak front [*He et al.*, 2011]. Another example is net upward pumping of nutrients at the shelfbreak by oscillating winds in the absence of an along-shelf pressure gradient [*Siedlecki et al.*, 2011]. However, the barotropic along-shelf pressure gradient associated with the along-shelf sea level tilt on the New England shelf strongly influences the structure of the shelfbreak jet and its associated secondary circulation (compare Figures 9a–9c and 11d–11f in *Zhang et al.* [2011]). Specifically, the along-shelf pressure gradient suppresses the onshore flow in the bottom boundary layer when there is westerly wind forcing. Consequently, inclusion of the along-shelf pressure gradient would diminish oscillation of near-bottom flow forced by oscillating winds and thereby dampen their effect on nutrient upwelling at the shelfbreak.

[51] Episodic events, including storms, onshore impinging of warm-core rings, and internal wave activity, may also have a large impact on mean biological production in the shelfbreak region. They can transport large amount of nutrients and other biological constituents through advection [*Marra et al.*, 1982] or redistribute the constituents swiftly through vertical and horizontal mixing [*Walsh et al.*, 1978]. As vertical diffusivity is a key factor in determining modeled mean biological production (section 3.4), it is imperative to understand how event-driven mixing affects the mean diffusivity. A good example is the substantial enhancement of mean diffusivity and doubling of the overall vertical heat flux by internal wave activity on the outer shelf off the coast of New Jersey [*Shroyer et al.*, 2010]. To quantify the contribution of episodic fluxes and mixing to the overall biological production in the shelfbreak region, high-resolution and long-term measurements and realistic modeling are required. We will investigate the issues in future studies using a 3-D model.

## 5. Conclusions

[52] To quantify the mean annual cycle of biological production in the vicinity of the southern New England shelfbreak, we compiled seasonal climatologies of MODIS surface chlorophyll data and historical in situ nutrient (nitrate and ammonium) and chlorophyll observations. Consistent patterns emerge in the cross-shelf and seasonal variations of chlorophyll: concentrations are generally higher on the inner- and mid-shelf and gradually decrease offshore, with highest concentrations in winter and lowest in summer. The satellite climatology shows slope-sea chlorophyll peaks in spring, presumably due to the spring bloom in the deep ocean. The in situ climatology reveals a distinct subsurface chlorophyll maximum in summer. Neither the satellite nor the in situ climatologies indicate significant enhancement of chlorophyll concentration near the shelfbreak, which is seemingly incompatible with the persistent shelfbreak upwelling predicted by a 2-D cross-shelf circulation model of the region.

[53] To investigate this apparent discrepancy, we implemented a four-component planktonic ecosystem model into a 2-D circulation model. The coupled model reproduces the major features in the climatological chlorophyll distribution, including the seasonal and cross-shelf variations and the summertime subsurface maximum. As in the climatologies, the model does not produce significant enhancement of chlorophyll concentration at the shelfbreak. However, it does predict local enhancement of biological productivity at the shelfbreak in spring and summer as a result of the persistently upwelled nutrient-rich slope water. Elevated zooplankton grazing at the shelfbreak prevents significant accumulation of phytoplankton biomass at the site of the upwelling. Sensitivity tests show that the model solutions are sensitive to vertical diffusivity and biological parameters, such as coefficients of the temperature regulation on phytoplankton and zooplankton growth rates, initial slope of the P-I curve, phytoplankton mortality rate and zooplankton-grazing coefficient.

[54] The simulations presented herein reflect one possible realization of the mean annual cycle of plankton productivity on the southern New England shelf and adjacent slope sea. In this model, top-down control by zooplankton grazing prevents significant enhancement of chlorophyll at the shelfbreak. This constitutes a testable hypothesis that will require simultaneous assessment of both bottom-up and top-down controls over seasonal time scales. Such a study would benefit from being couched within the Ocean Observatories Initiative Pioneer Array, not only because of the long-term nature of the expected deployment, but also because of the high-resolution measurements in both the cross-shore and along-shore directions near the front.

[55] Improved observational capabilities will also set the stage for more realistic modeling of 3-D processes at the shelfbreak front. Indeed, the mechanisms underlying the enhancement of chlorophyll sometimes observed in synoptic realizations of the front remain obscure. Linkage of observations with models in a 3-D synoptic context provides an exceptional opportunity for the study of such processes, particularly in light of recent advances in the assimilation of both physical [*Moore et al.*, 2011; *Zhang et al.*, 2010] and biological data [*Gregg et al.*, 2009].

## Appendix A: Sensitivity to Model Biological Parameters

[56] We conducted a series of sensitivity tests by perturbing each parameter in Table 1 by ±50% and comparing the solutions to the baseline seasonal simulations (referred to as control runs hereafter). We chose the cross-shelf distribution of chlorophyll (Figure 4) to be the comparison metric (Figures A1, A2, A3). The results are summarized as follows:

[57] 1. The effects of adjusting reference temperature, $T_0$, are complex because this parameter appears in both the phytoplankton growth rate ($U$) and the zooplankton grazing
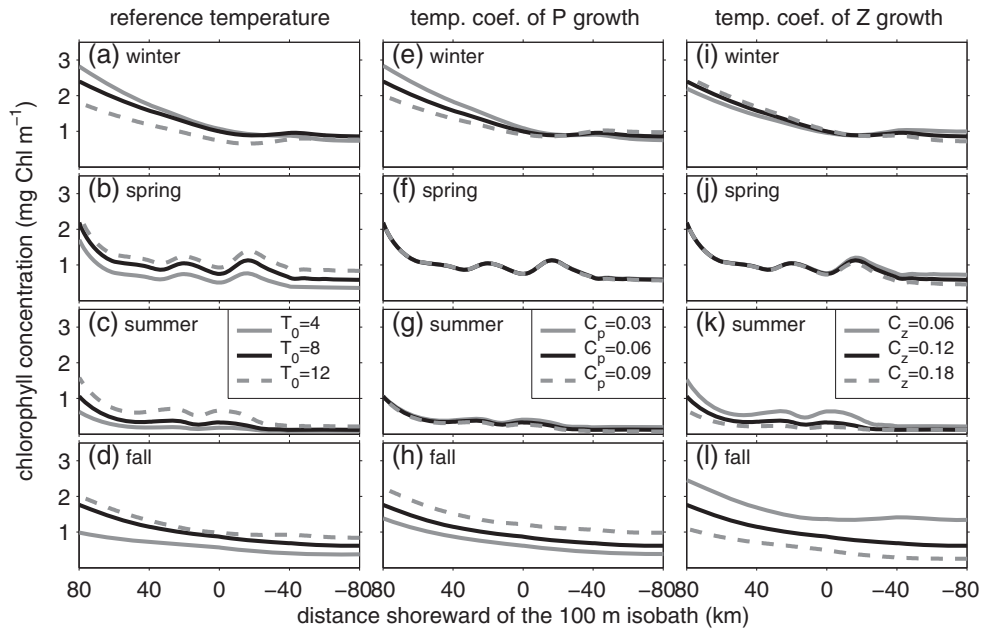
**Figure A1.** Sensitivity of the chlorophyll concentration to the reference temperature (left column) and temperature coefficients of phytoplankton (middle column) and zooplankton (right column) growth.

rate ($G$). Halving $T_0$ increases (decreases) wintertime chlorophyll inshore (offshore) (Figure A1a). In all other seasons, halving $T_0$ reduces chlorophyll both inshore and offshore (Figures A1b–A1d). As shown in Figure A4a, reducing $T_0$ increases the temperature-dependent factor in both $U$ and $G$; the relative magnitude of these two terms determines whether the perturbation to $T_0$ will increase or decrease phytoplankton abundance. Specifically, grazing plays a lesser role in controlling the phytoplankton population in winter than it does in other seasons (Figures 11e–11h). As such, wintertime

phytoplankton production increases more than zooplankton grazing does—and as a result the abundance of phytoplankton increases. Conversely, in other seasons the proportional increase in grazing overshadows that of phytoplankton production, thereby reducing phytoplankton abundance in spring, summer, and fall.

[58] 2. Adjusting the temperature coefficient of phytoplankton growth, $C_p$, changes the phytoplankton concentration in winter and fall, but not in spring and summer (Figures A1e–A1h). The lack of a response in spring and
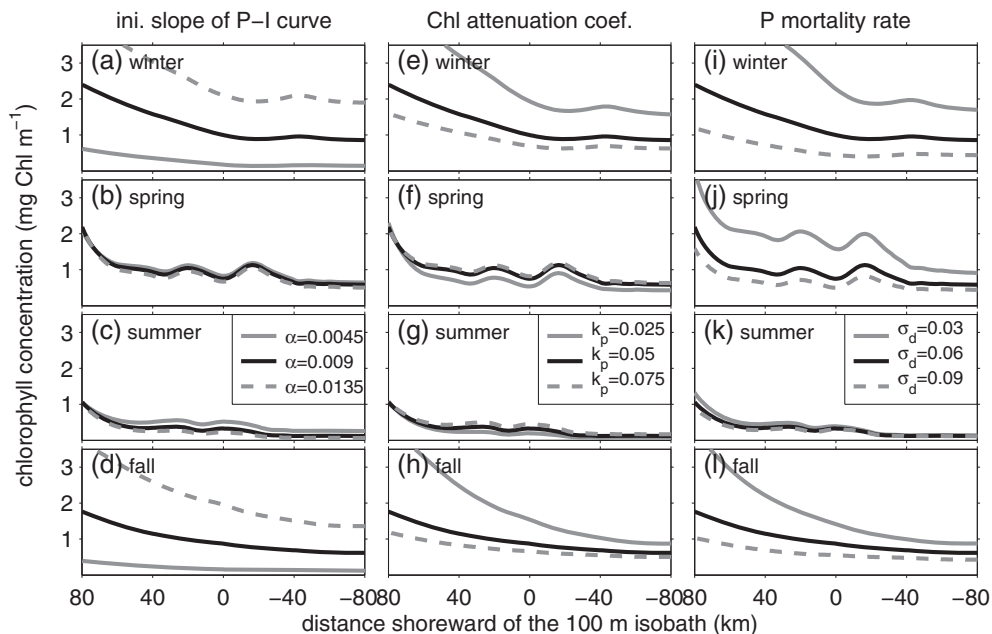


**Figure A2.** Sensitivity of the chlorophyll concentration to initial slope of the P-I curve (left column), chlorophyll light attenuation coefficient (middle column), and phytoplankton mortality rate (right column).
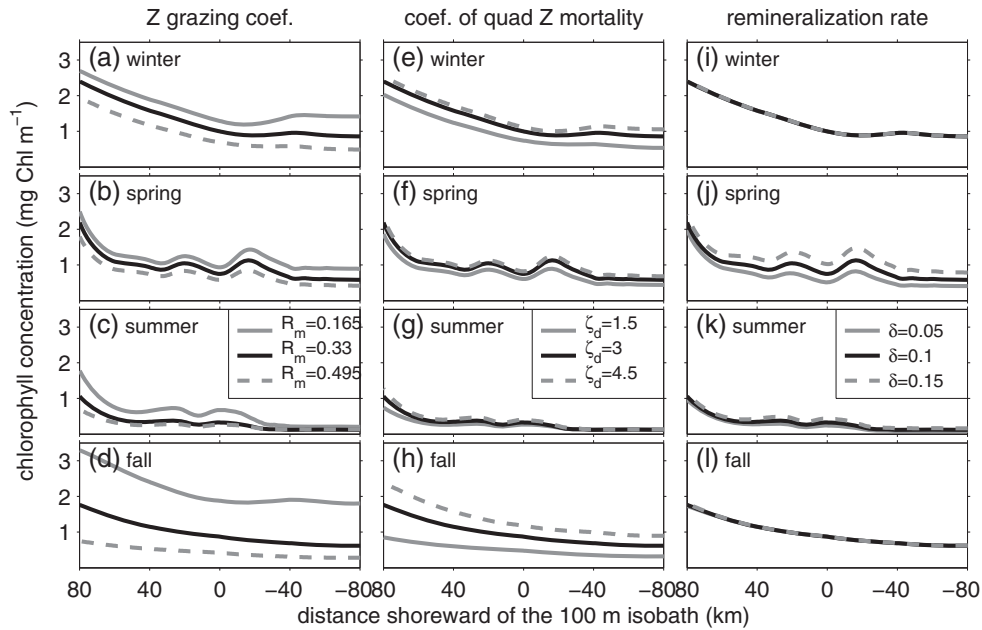
**Figure A3.** Sensitivity of the chlorophyll concentration to zooplankton-grazing coefficient (left column), coefficient of the quadratic zooplankton mortality term (middle column), and remineralization rate (right column).

summer reflects the role of nutrient limitation in suppressing phytoplankton growth (equation (6)). Extremely low $N$ limits the extent $U$ can vary in response to changes in $C_p$. Reducing $C_p$ increases wintertime phytoplankton concentrations onshore and decreases them offshore. This is caused by the opposite effects of changing $C_p$ on $U$ at temperatures lower and higher than $T_0$ (8°C in this case; Figure A4b). For water colder than 8°C, which is onshore of the

shelfbreak in winter (Figure 2a), reducing $C_p$ increases $U$ and therefore enhances phytoplankton abundance. The opposite holds for water warmer than 8°C, which is present offshore of the shelfbreak in winter. In the fall, the entire domain is warmer than 8°C, and so decreasing $C_p$ causes phytoplankton abundance to drop throughout the model domain.

[59] 3. Adjusting the temperature coefficient of zooplankton grazing, $C_z$, changes phytoplankton concentrations most dramatically in the fall (Figures A1i–A1l). Because water temperatures are higher than 8°C throughout the model domain during that season, decreasing $C_z$ decreases the grazing rate (Figure A4b) and therefore increases phytoplankton abundance. The effect is similar in summer, but to a lesser extent. The reduced variability is a consequence of the phytoplankton maximum occurring at depth, where it is less detectable via remote sensing. In winter, reducing $C_z$ has opposite effects on phytoplankton abundance inshore versus offshore of the shelfbreak because of the aforementioned temperature gradient. Specifically, temperatures colder than 8°C onshore of the shelfbreak cause a decrease in $C_z$ to increase $G$ (Figure A4b) and thereby decrease phytoplankton. The opposite occurs in the warmer water offshore of the shelfbreak in winter. In spring, adjusting $C_z$ does not change phytoplankton concentration onshore of the shelfbreak because the surface water is close to 8°C (Figure 2b) and varying $C_z$ there does not change $G$ (Figure A4b).

[60] 4. Increasing the initial slope of the photosynthesis versus irradiance (P-I) curve, $\alpha$, (Figures A2a–A2d) increases phytoplankton concentration in winter and fall by increasing the efficiency of light utilization at a time when production is light limited. In nutrient-limited conditions of the spring and summer, increasing $\alpha$ tends to deepen the euphotic zone, thereby causing chlorophyll to accumulate deeper in the water
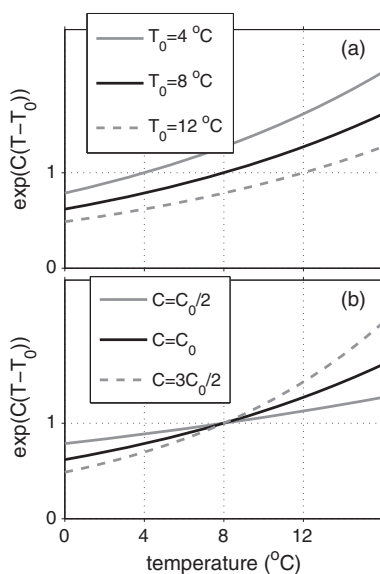


**Figure A4.** Changes of the exponential function to different values of (a) reference temperature and (b) temperature coefficient.

column. This in turn lessens the amount of chlorophyll detectable via remote sensing. Adjusting the biologically active portion of shortwave radiation, $\beta$, generates similar effects (not shown).

[61] 5. Adjusting the chlorophyll attenuation coefficient, $k_p$, changes the influence of phytoplankton on the underwater light field, thereby generating the opposite effects as adjusting $\alpha$ (Figures A2e–A2h).

[62] 6. Increasing or decreasing the nutrient uptake rate, $V_m$, and the half saturation constant, $k_N$, by 50% has little effect on the seasonal phytoplankton concentrations (not shown). Applying the parameter values in Table 1 and the modeled nutrient and phytoplankton concentrations in equations (6) and (8) gives $\alpha I \ll V_m$ and $k_N \ll N$ for all cases, which means $V_m/(V_m^2 + \alpha^2 I^2)^{1/2} \approx 1$ and $N/(k_N + N) \approx 1$ in equation (6). Hence, changing $V_m$ or $k_N$ by 50% does not change the relationship and has therefore little effect on $U$.

[63] 7. Changing the value of the phytoplankton mortality rate, $\sigma_d$, by 50% changes phytoplankton concentration substantially in winter, spring, and fall, but relatively little in summer (Figures A2i–A2l). The relatively small change in summer is mainly caused by low detectability of the subsurface chlorophyll variation via remote sensing.

[64] 8. Increasing the zooplankton-grazing coefficient, $R_m$, increases grazing and reduces phytoplankton concentrations in all seasons (Figures A3a–vd), but the effect is relatively small in summer because the phytoplankton population resides mostly at depth, as previously stated. Adjusting the Ivlev constant, $\Lambda$, has a similar effect (not shown).

[65] 9. Increasing the coefficient of quadratic zooplankton mortality, $\zeta_d$, decreases zooplankton concentration and increases the phytoplankton concentration in all seasons (Figures A3e–A3h). The opposite effect is achieved by adjusting zooplankton assimilation efficiency, $\gamma$ (not shown).

[66] 10. Adjusting the detritus remineralization rate, $\delta$, and sinking velocity, $w_d$, affects the distribution of nutrients in the water column. During the fall and winter seasons in which primary production is light limited, variations in $\delta$ or $w_d$ have no effect on phytoplankton concentration (see Figures A3i–A3l for the effect of adjusting $\delta$). Increasing $\delta$ or decreasing $w_d$ increases the availability of nutrients in the euphotic zone and therefore increases the phytoplankton population in spring and summer.

## Appendix B: Effects of Vertical Diffusivity

[67] To quantify the effects of vertical diffusivity, two additional series of seasonal simulations were conducted with the imposed surface and bottom mixed layers removed separately (Figure B1). In those simulations, vertical diffusivity given by the GLS *k-kl* type turbulence closure (Figure 7a) was used. As described in section 2.1.3 above, vertical diffusivity profiles given by the turbulence closure scheme contain much thinner mixed layers (~15 and 10 m in winter, ~8 and 5 m in spring, ~7 and 3 m in summer, and ~12 and 3 m in fall at the shelfbreak for surface and bottom mixed layers, respectively) relative to the climatological MLDs (Figure 6).

[68] Deepening the surface mixed layer has two competing effects on phytoplankton production: it can (1) suppress phytoplankton growth by limiting the average light level to which the phytoplankton is exposed and (2) stimulate growth by entraining more nutrients into the euphotic zone. We expect the first effect to be dominant in winter and fall when the phytoplankton population is light limited. The second effect should be more pronounced in spring and summer when nutrient availability limits primary production. Replacement of the climatological mean mixed layers with the turbulence closure model confirms this (Figure B1). The model generates a much stronger surface phytoplankton bloom in winter and fall because the shallower mixed layer lessens light limitation. The phytoplankton population is lower in spring and summer due to less nutrient availability.
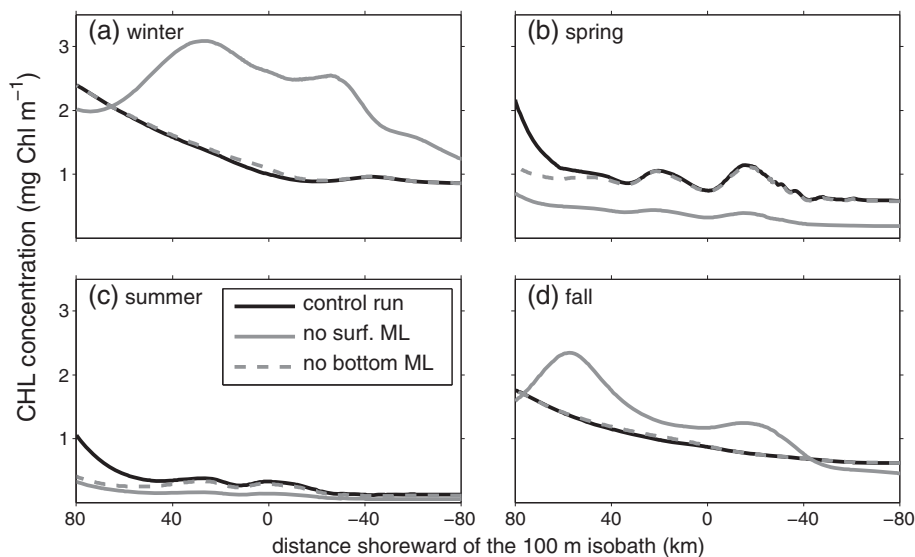


**Figure B1.** Cross-shelf distribution of chlorophyll concentration calculated from the control simulations (black lines) and the simulations without the thickened surface (solid grey lines) and bottom (dashed grey lines) mixed layers.

Removal of the bottom mixed layers has only a modest impact on the solutions. In the nearshore region, the proximity of the bottom mixed layer to the euphotic zone makes it a potential source of nutrients. Therefore, the absence of the bottom mixed layer causes a reduction in phytoplankton in the nearshore areas during the nutrient-limited seasons (spring and summer).

# References

Barth, J. A., D. Bogucki, S. D. Pierce, and P. M. Kosro (1998), Secondary circulation associated with a shelfbreak front, *Geophys. Res. Lett.*, *25*, 2761–2764.

Biscaye, P. E., and R. F. Anderson (1994), Fluxes of particulate matter on the slope of the southern Middle Atlantic Bight: SEEP-II, *Deep-Sea Res. II*, *41*(2-3), 459–509.

Brush, M. J., J. W. Brawley, S. W. Nixon, and J. N. Kremer (2002), Modeling phytoplankton production: Problems with the Eppley curve and an empirical alternative, *Mar. Ecol. Prog. Ser.*, *238*, 31–45.

CETAP (1982), A characterization of marine mammals and turtles in the Mid- and North-Atlantic areas of the U.S. outer continental shelf, *Cetacean and Turtle Assessment Program Rep.*, 77 pp, University of Rhode Island, Kingston, Rhode Island.

Chapman, D. C. (1985), Numerical treatment of cross-shelf open boundaries in a barotropic ocean model, *J. Phys. Oceanogr.*, *15*, 1060–1075.

Consortium for Ocean Leadership (2010), Ocean observatories initiative: Final network design, *Rep. 1101-00000*, 170 pp, Washington DC.

Cullen, J. J. (1982), The deep chlorophyll maximum: Comparing vertical profiles of chlorophyll a, *Can. J. Fish. Aquat. Sci.*, *39*, 791–803.

Durbin, E. G., and A. G. Durbin (1996), Zooplankton dynamics in the northeast shelf ecosystem, in *The Northeast Shelf Ecosystem: Assessment, Sustainability, and Management*, edited by K. Sherman, N. A. Jaworski and T. J. Smayda, pp. 129–152, Blackwell Science, Cambridge, Massachusetts, USA.

Edwards, A. M., and J. Brindley (1996), Oscillatory behaviour in a three-component plankton population model, *Dynamics and Stability of Systems*, *11*(4), 347–370.

Eppley, R. W. (1972), Temperature and phytoplankton growth in the sea, *Fish. Bull.*, *70*, 1063–1085.

Fasham, M. J. R. (1995), Variations in the seasonal cycle of biological production in subarctic oceans: A model sensitivity analysis, *Deep-Sea Res. I*, *42*(7), 1111–1149.

Fennel, K., M. Losch, J. Schroter, and M. Wenzel (2001), Testing a marine ecosystem model: Sensitivity analysis and parameter optimization, *J. Mar. Syst.*, *28*, 45–63.

Fennel, K., J. Wilkin, J. Levin, J. Moisan, J. O'Reilly, and D. Haidvogel (2006), Nitrogen cycling in the Middle Atlantic Bight: Results from a three-dimensional model and implications for the North Atlantic nitrogen budget, *Global Biogeochem. Cy.*, *20*(GB3007).

Flagg, C. N., C. D. Wirick, and S. L. Smith (1994), The internaction of phytoplankton, zooplankton and currents from 15 months of continuous data in the Mid-Atlantic Bight, *Deep-Sea Res. II*, *41*(2/3), 411–435.

Flather, R. A. (1976), A tidal model of the northwest European continental shelf, *Mem. Soc. Roy. Sci. Liege, Ser. 6*, (10), 141–164.

Fleming, N. E., and J. L. Wilkin (2010), MOCHA: A 3-D climatology of the temperature and salinity of the Middle Atlantic Bight, *Eos Trans. AGU*, *91*(26), Ocean Sci. Meet. Suppl.

Friedrichs, M. A. M., et al. (2007), Assessment of skill and portability in regional marine biogeochemical models: Role of multiple planktonic groups, *J. Geophys. Res.*, *112*, C08001.

Gamble, J. C. (1978), Copepod grazing during a declining spring phytoplankton bloom in the northern North Sea, *Mar. Biol.*, *49*, 303–315.

Gawarkiewicz, G., K. H. Brink, F. Bahr, R. C. Beardsley, M. Caruso, J. Lynch, and C.-S. Chiu (2004), A large-amplitude meander of the

shelfbreak front in the Middle Atlantic Bight: Observations from the Shelfbreak PRIMER Experiment, *J. Geophys. Res.*, *109*(C03006), doi:10.1029/2002JC001468.

Gregg, W. W., M. A. M. Friedrichs, A. R. Robinson, K. A. Rose, S. Reiner, K. R. Thompson, and S. C. Doney (2009), Skill assessment in ocean biological data assimilation, *J. Mar. Syst.*, *76*(1-2), 16–33.

Hales, B., R. D. Vaillancourt, L. Prieto, J. Marra, R. Houghton, and D. Hebert (2009), High-resolution surveys of the biogeochemistry of the New England shelfbreak front during summer, 2002, *J. Mar. Syst.*, *78*(3), 426–441.

He, R., K. Chen, K. Fennel, G. G. Gawarkiewicz, and D. J. McGillicuddy (2011), Seasonal and interannual variability of physical and biological dynamics at the shelfbreak front of the Middle Atlantic Bight: Nutrient supply mechanisms, *Biogeosciences*, *8*, 2935–2946.

Hirst, A. G., and A. J. Bunker (2003), Growth of marine planktonic copepods: Global rates and patterns in relation to chlorophyll a, temeperature, and body weight, *Limnol. Oceanogr.*, *48*(5), 1988–2010.

Hofmann, E. E., et al. (2011), Modeling the dynamics of continental shelf carbon, *Annual Review of Marine Science*, *3*, 93–122.

Houghton, R. W., and J. Marra (1983), Physical/biological structure and exchange across the thermohaline shelf/slope front in the New York Bight, *J. Geophys. Res.*, *88*(C7), 4467–4481.

Houghton, R. W., D. Hebert, and M. Prater (2006), Circulation and mixing at the New England shelfbreak front: Results of purposeful tracer experiments, *Progr. Oceanogr.*, *70*(2-4), 289–312.

Houghton, R. W., R. D. Vaillancourt, J. Marra, D. Hebert, and B. Hales (2009), Cross-shelf circulation and phytoplankton distribution at the summertime New England shelfbreak front, *J. Mar. Syst.*, *78*(3), 411–425.

Huntley, M. E., and M. D. G. Lopez (1992), Temperature-dependent production of marine copepods: A global synthesis, *Amer. Nat.*, *140*(2), 201–242.

Judkins, D. C., C. D. Wirick, and W. E. Esaias (1980), Composition, abundance, and distribution of zooplankton in the New York Bight, September 1974–September 1975, *Fish. Bull.*, *77*(3), 669–683.

Kirk, J. T. O. (1994), Light and Photosynthesis in Aquatic Ecosystems, 2 ed., 528 pp., Cambridge University Press, New York.

Ledwell, J., T. F. Duda, M. Sundermeyer, and H. Seim (2004), Mixing in a coastal environment: 1. A view from dye dispersion, *J. Geophys. Res.*, *109*, C10013.

Lentz, S. J. (2008), Observations and a model of the mean circulation over the Middle Atlantic Bight continental shelf, *J. Phys. Oceanogr.*, *38*(6), 1203–1221.

Linder, C. A., and G. Gawarkiewicz (1998), A climatology of the shelfbreak front in the Middle Atlantic Bight, *J. Geophys. Res.*, *103*, 18,405–418,423.

MacKinnon, J. A., and M. C. Gregg (2003), Mixing on the late-summer New England Shelf—Solibores, shear, and stratification, *J. Phys. Oceanogr.*, *33*, 1476–1492.

MacKinnon, J. A., and M. C. Gregg (2005), Spring mixing: Turbulence and internal waves during restratification on the New England shelf, *J. Phys. Oceanogr.*, *35*, 2425–2443.

Malone, T. C., T. S. Hopkins, P. G. Falkowski, and T. E. Whitledge (1983), Production and transport of phytoplankton biomass over the continental shelf of the New York Bight, *Cont. Shelf Res.*, *1*(4), 305–337.

Marra, J., R. W. Houghton, and C. Garside (1990), Phytoplankton growth at the shelf-break front in the middle Atlantic Bight, *J. Mar. Res.*, *48*, 851–868.

Marra, J., R. W. Houghton, D. C. Boardman, and P. J. Neale (1982), Variability in surface chlorophyll a at a shelf-break front, *J. Mar. Res.*, *40*, 575–591.

McGillicuddy, D. J., J. J. McCarthy, and A. R. Robinson (1995), Coupled physical and biological modeling of the spring bloom in the North Atlantic (I): Model formulation and one dimensional bloom processes, *Deep-Sea Res. I*, *42*(8), 1313–1357.

Moore, A. M., H. G. Arango, G. Broquet, B. S. Powell, A. T. Weaver, and J. Zavala-Garay (2011), The Regional Ocean Modeling System (ROMS) 4-dimensional variational data assimilation systems: I—System overview and formulation, *Progr. Oceanogr.*, *91*, 34–49.

Mousseau, L., L. Legendre, and L. Fortier (1996), Dynamics of size-fractionated phytoplankton and trophic pathways on the Scotian Shelf and at the shelf break, Northwest Atlantic, *Aquat. Microb. Ecol.*, *10*, 149–163.

O'Reilly, J. E., and C. Zetlin (1998), Season, horizontal, and vertical distribution of phytoplankton chlorophyll a in the northeast U.S. continental shelf ecosystem, *NOAA Technical Rep. NMFS 139*, 119 pp, NOAA, U.S. Department of Commerce, Seattle, Washington.

Orlanski, I. (1976), A simple boundary condition for unbounded hyperbolic flows, *J. Comput. Phys.*, *21*, 251–269.

Orphanides, C. D., and G. M. Magnusson (2007), Characterization of the Northeast and Mid-Atlantic bottom and mid-water trawl fisheries based on Vessel Trip Report (VTR) data, *Northeast Fisheries*

*Science Center Reference Documents Rep. 07-15*, 127 pp, National Marine Fisheries Service, NOAA, U.S. Department of Commerce, Woods Hole, MA.

Paffenhöfer, G.-A. (1971), Grazing and ingestion rates of nauplii, copepodids and adults of the marine planktonic copepod *Calanus helgolandicus*, *Mar. Biol.*, *11*, 286–298.

Pickart, R. S. (2000), Bottom boundary layer structure and detachment in the shelfbreak jet of the Middle Atlantic Bight, *J. Phys. Oceanogr.*, *30*(11), 2668–2686.

Podesta, G. P., J. A. Browder, and J. J. Hoey (1993), Exploring the association between swordfish catch rates and thermal fronts on U.S. longline grounds in the western North Atlantic, *Cont. Shelf Res.*, *13*(2-3), 253–277.

Powell, T. M., C. V. W. Lewis, E. N. Curchitser, D. B. Haidvogel, A. J. Hermann, and E. L. Dobbins (2006), Results from a three-dimensional, nested biological-physical model of the California Current System and comparisons with statistics from satellite imagery, *J. Geophys. Res.*, *111*(C07018), doi:10.1029/2004JC002506.

Rehmann, C. R., and T. F. Duda (2000), Diapycnal diffusivity inferred from scalar microstructure measurements near the New England shelf/slope front, *J. Phys. Oceanogr.*, *30*, 1354–1371.

Riley, G. A. (1942), The relationship of vertical turbulence and spring diatom flowerings, *J. Mar. Res.*, *5*(1), 67–87.

Rose, J. M., and D. A. Caron (2007), Does low temperature constrain the growth rates of heterotrophic protists? Evidence and implications for algal blooms in cold waters, *Limnol. Oceanogr.*, *52*(2), 886–895.

Ryan, J. P., J. A. Yoder, and P. C. Cornillon (1999a), Enhanced chlorophyll at the shelfbreak of the Mid-Atlantic Bight and Georges Bank during the spring transition, *Limnol. Oceanogr.*, *44*(1), 1–11.

Ryan, J. P., J. A. Yoder, J. A. Barth, and P. C. Cornillon (1999b), Chlorophyll enhancement and mixing associated with meanders of the shelf break front in the Mid-Atlantic Bight, *J. Geophys. Res.*, *104*(C10), 23479–23493.

Shchepetkin, A. F., and J. C. McWilliams (2008), Computational kernel algorithms for fine-scale, multiprocess, long-term oceanic simulations, in Handbook of Numerical Analysis. XIV: Computational Methods for the Ocean and the Atmosphere, edited by P. G. Ciarlet, T. Temam and J. Tribbia, pp. 119–182, Elsevier Science, Oxford, U. K.

Sherman, K., N. A. Jaworski, and T. J. Smayda (1996a), The Northeast Shelf Ecosystem: Assessment, Sustainability and Management, Blackwell Science, Cambridge, Massachusetts, USA.

Sherman, K., A. Solow, J. Jossi, and J. Kane (1998), Biodiversity and abundance of the zooplankton of the Northeast Shelf ecosystem, *ICES J. Mar. Sci.*, *55*, 730–738.

Sherman, K., J. Kane, S. Murawski, W. Overholtz, and A. Solow (2002), The U.S. northeast shelf large marine ecosystem: Zooplankton trends in fish biomass recovery, in *Large Marine Ecosystems of the North Atlantic*: *Changing States and Sustainability*, edited by K. Sherman and H. R. Skjoldal, pp. 195–215, Elsevier Science B.V., Amsterdam, The Netherlands.

Sherman, K., M. Grosslein, D. Mountain, D. Busch, J. O'Reilly, and R. Theroux (1996b), The northeast shelf ecosystem: an initial prospective, in The Northeast Shelf Ecosystem: Assessment, Sustainability, and Management, edited by K. Sherman, N. A. Jaworski and T. J. Smayda, pp. 103–126, Blackwell Science, Cambridge, Massachusetts, USA.

Shigemitsu, M., T. Okunishi, J. Nishioka, H. Sumata, T. Hashioka, M. N. Aita, S. L. Smith, N. Yoshie, N. Okada, and Y. Yamanaka (2012), Development of a one-dimensional ecosystem model including the iron cycle applied to the Oyashio region, western subarctic Pacific, *J. Geophys. Res.*, *117*, C06021.

Shroyer, E. L., J. N. Moum, and J. D. Nash (2010), Vertical heat flux and lateral mass transport in nonlinear internal waves, *Geophys. Res. Lett.*, *37*, L08601.

Siedlecki, S. A., D. E. Archer, and A. Mahadevan (2011), Modeling mechanisms for nutrient supply and ventilation of benthic gases at the continental shelf break, *J. Geophys. Res.*, *116*, C06023.

Siegel, D. A., S. Maritorena, N. B. Nelson, and M. J. Behrenfeld (2005), Independence and interdependencies among global ocean color properties: Reassessing the bio-optical assumption, *J. Geophys. Res.*, *110*, C07011.

Smith, R. C. (1981), Remote sensing and depth distribution of ocean chlorophyll, *Mar. Ecol. Prog. Ser.*, *5*, 359–361.

Smith, S. L., and P. V. Z. Lane (1988), Grazing of the spring diatom bloom in the New York Bight by the calanoid copepods *Calanus finmarchicus*, *Metridia lucens* and *Centropages typicus*, *Cont. Shelf Res.*, *8*, 485–509.

Steele, J., and E. W. Henderson (1981), A simple plankton model, *Amer. Nat.*, *117*, 676–691.

Umlauf, L., and H. Burchard (2003), A generic length-scale equation for geophysical turbulence models, *J. Mar. Res.*, *61*, 235–265.

Vaillancourt, R. D., J. Marra, L. Prieto, R. W. Houghton, B. Hales, and D. Hebert (2005), Light absorption and scattering by particles and CDOM at the New England shelfbreak front, *Geochem., Geophys., Geosyst.*, *6*, Q11003.

Walsh, J. J., P. E. Biscaye, and G. T. Csanady (1988a), The 1983–1984 shelf edge exchange processes (SEEP)—I experiment: Hypotheses and highlights, *Cont. Shelf Res.*, *8*(5-7), 435–456.

Walsh, J. J., T. E. Whitledge, F. W. Barvenik, C. D. Wirick, and S. O. Howe (1978), Wind events and food chain dynamics within the New York Bight, *Limnol. Oceanogr.*, *23*(4), 659–683.

Walsh, J. J., C. D. Wirick, L. J. Pietrafesa, T. E. Whitledge, F. E. Hoge, and R. N. Swift (1988b), High-frequency sampling of the 1984 spring bloom within the Mid-Atlantic Bight: Synoptic shipboard, aircraft, and in situ perspectives of the SEEP-I experiment, *Cont. Shelf Res.*, *8*, 529–563.

Walsh, J. J., et al. (2005), A numerical model of seasonal primary production within the Chukchi/Beaufort Seas, *Deep-Sea Res. II*, *52*, 3541–3576.

Warner, J. C., C. R. Sherwood, H. G. Arango, R. P. Signell, and B. Butman (2005), Performance of four turbulence closure models implemented using a generic length scale method, *Ocean Model.*, *8*, 81–113.

White, J. R., and M. R. Roman (1992), Seasonal study of grazing by metazoan zooplankton in the mesohaline Chesapeake Bay, *Mar. Ecol. Prog. Ser.*, *86*, 251–261.

Wroblewski, J. S. (1977), A model of phytoplankton plume formation during variable Oregon upwelling, *J. Mar. Res.*, *35*, 357–394.

Xu, Y., R. J. Chant, D. Gong, R. Castelao, S. M. Glenn, and O. Schofield (2011), Seasonal variability of chlorophyll a in the Mid-Atlantic Bight, *Cont. Shelf Res.*, *31*, 1640–1650.

Yoder, J. A., S. E. Schollaert, and J. E. O'Reilly (2002), Climatological phytoplankton chlorophyll and sea surface temperature patterns in continental shelf and slope waters off the northeast U.S. coast, *Limnol. Oceanogr.*, *47*(3), 672–682.

Yoder, J. A., J. E. O'Reilly, A. H. Barnard, T. S. Moore, and C. M. Ruhsam (2001), Variability in coastal zone color scanner (CZCS) chlorophyll imagery of ocean margin waters off the US East Coast, *Cont. Shelf Res.*, *21*, 1191–1218.

Zhang, W. G., J. L. Wilkin, and H. G. Arango (2010), Towards an integrated observation and modeling system in the New York Bight using variational methods, part I: 4DVAR data assimilation, *Ocean Model.*, *35*(3), 119–133.

Zhang, W. G., G. G. Gawarkiewicz, D. J. McGillicuddy, and J. L. Wilkin (2011), Climatological mean circulation at the New England shelf break, *J. Phys. Oceanogr.*, *41*, 1874–1893.